Characterization of effector binding preferences between oncogenic mutants KRAS4b G12D and KRAS4b G12C

By

Megan Rigby

B.A. Biology (St. Mary's College of Maryland) 2015

THESIS

Submitted in partial satisfaction of the requirements for the degree of

MASTER OF SCIENCE

In

BIOMEDICAL SCIENCE

In the

GRADUATE SCHOOL

Of

HOOD COLLEGE

November 2022

Accepted:

_____	_____
Ann L Boyd, Ph.D. Committee Member	Meredith Yeager, Ph.D. Director, Biomedical Science Program
_____	
Craig Laufer, Ph.D. Committee Member	
_____	_____
Thomas Turbyville, Ph.D. Thesis Adviser	April M. Boulton, Ph.D. Dean of the Graduate School

STATEMENT OF USE AND COPYRIGHT WAIVER

I authorize Hood College to lend this thesis, or reproductions of it, in total or part, at the request of other institutions or individuals for the purpose of scholarly research.

ACKNOWLEDGEMENTS

This work was completed at the RAS Initiative at the Frederick National Laboratory for Cancer Research under the direction of Dr. Anna Maciag and Dr. Thomas Turbyville. I am sincerely grateful for their technical guidance, encouragement, and support. They have shaped my growth as a scientist and as a person, and I am lucky to have such knowledgeable and supportive mentors.

I would also like to thank John Columbus, Brian Smith, and Nicole Fer for their training and advice regarding cell culture, transfections, BRET, and general lab lore. I would like to acknowledge and thank Vanessa Wall and Dr. Dominic Esposito for generating the plasmids used in this project, and William Burgan and Katie Powell for generating the cell lines. I would like to thank Brian Smith for his contribution of data in Figure 16. Thank you to Dr. Alok Sharma for generously providing the protein NMR data and expertise, and to Dr. Vandana Kumari for her molecular dynamics simulations. I'm grateful to Dr. Trent Balius for sharing his knowledge of RAS structural data, and for his guidance on using Chimera software. Finally, thank you to Conor Jenkins for his advice on statistical analysis, normalization, and much needed emotional support and love.

TABLE OF CONTENTS

ABSTRACT

Up to 30% of cancers harbor mutations in the small GTPase *RAS* that maintain the protein in an active conformation and drive uncontrolled cellular proliferation, promote cell survival, and alter cellular metabolism, movement, and differentiation. The momentum of four decades of research is finally yielding promising results in targeting this previously deemed 'undruggable' protein. However, much remains to be understood about fundamental RAS biology and signaling. For instance, it is still unclear why specific mutations occur with non-uniform frequency across cancer types. Do RAS mutants differ in their ability to engage effector proteins and potentiate signaling pathways? Here, we optimize a cellular Bioluminescence Resonance Energy Transfer (BRET) system to help answer this question, and use BRET Saturation curves and immunoprecipitation to interrogate the ability of common mutants KRAS4b G12D and KRAS4b G12C to engage with effectors RAF1 and p110α. We were unable to identify significant differences in effector affinity with BRET saturation curves, but did find greater p110α engagement by KRAS4b G12D through GFP pull-downs in doxycycline-inducible GFP-KRAS mutant HeLa cell lines as well as transiently transfected HEK293T cells. We also observed higher AKT phosphorylation in KRAS G12D-driven HeLa and oncogenic cell lines, suggesting greater levels of PI3K pathway activation in cells carrying this mutation. We then discuss our solution-state NMR and molecular dynamics simulation studies revealing structural differences in the KRAS4b G12D protein, and how these differences may influence effector engagement and oncogenic signaling.

LIST OF TABLES

LIST OF FIGURES

LIST OF ABBREVIATIONS

BRET	Bioluminescence resonance energy transfer
CRC	Colorectal cancer
CRD	Cysteine-rich domain
CSP	Chemical shift perturbation
GAP	GTP-ase activating protein
GDP	Guanine diphosphate
GEF	Guanine nucleotide exchange factor
GTP	Guanine triphosphate
HVR	Hypervariable region
HSQC	Heteronuclear single quantum coherence
MDS	Molecular dynamics simulations
NMR	Nuclear magnetic resonance
NOE	Nuclear Overhauser effect
NSCLC	Non-small cell lung cancer
PDAC	Pancreatic ductal adenocarcinoma
PI3K	Phosphatidylinositol-4,5-bisphosphate 3-kinase
RBD	RAS binding domain

RBDCRD	RAS binding domain and cysteine rich domain. RAF1 residues 52-188
RMSD	Root-mean-squared displacement
RMSF	Root-mean-squared fluctuation

INTRODUCTION

RAS proteins act as molecular switches

RAS proteins were the first members identified of a highly conserved large superfamily of GTPases, of which over 150 have since been discovered (Takai et al., 2001). Three *RAS* genes (*HRAS, NRAS,* and *KRAS*) encode a total of four protein products: HRAS, NRAS, and the splice variants KRAS4a and KRAS4b. Acting from the inner leaflet of the plasma membrane, these proteins serve as molecular switches, transducing extracellular signals and conducting a symphony of complex signaling pathways that result in proliferation, differentiation, movement, metabolism, and cell survival (Pearson et al., 2001; Ferro and Trabalzini, 2010; Castellano and Downward, 2011). Mutations that keep RAS in an active state are among the most common drivers of cancer (Simanshu et al., 2017).

RAS proteins are comprised of a globular (G) domain (residues 1-166), where nucleotide binding and effector engagement occur, and a disordered, c-terminal tail (residues 166-188/189) (Simanshu et al., 2017). Each of the four isoforms are identical across the first 86 residues (termed the effector lobe), show slight differences in residues 87-166 (the allosteric lobe), and diverge significantly across their c-terminal tail sequences, aptly named the ‘hypervariable region’, or HVR (Gasper and Wittinghofer, 2020).

RAS cycles between active, guanosine triphosphate (GTP)-bound and inactive, guanosine diphosphate (GDP)-bound states. Under normal signaling conditions, activation is mediated by guanine nucleotide exchange factors (GEFs) and GTP-ase

activating proteins (GAPs), which are recruited to the inner plasma membrane upon cellular receptor stimulation by extracellular ligands (Bos et al., 2007) (Figure 1). GEFs catalyze the release of GDP, which is quickly replaced by the more highly abundant GTP, for which it also has a greater affinity (Hunter et al., 2015). RAS's intrinsic hydrolytic activity is significantly stimulated by GAPs, leading to the ejection of a phosphate and protein deactivation (Bos et al., 2007). When bound to GTP, RAS adopts a conformational state that promotes interaction with a multitude of effector molecules. The two most relevant RAS effectors to oncogenesis are RAF1 kinase and phosphatidylinositol-4,5-bisphosphate 3-kinase (PI3K) (Figure 1).

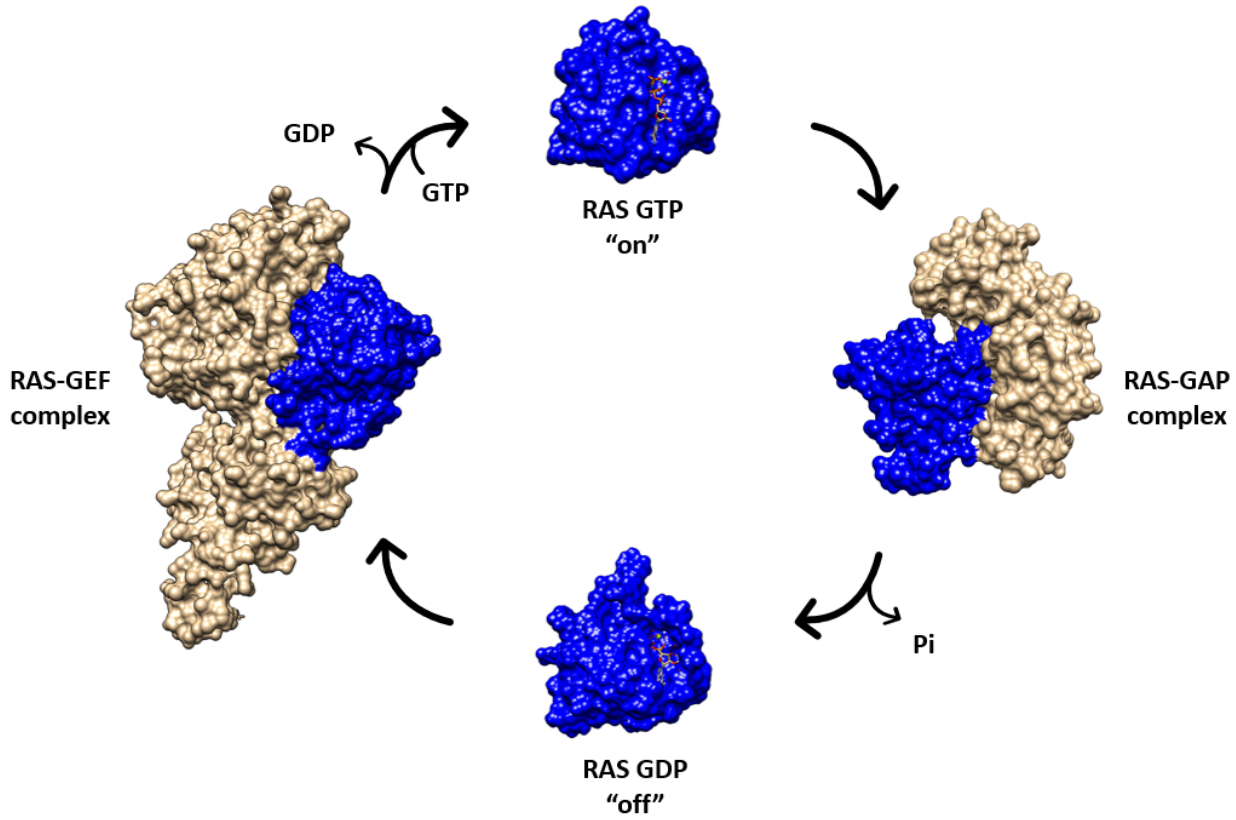

Figure 1. **RAS nucleotide cycling.** In healthy tissue, RAS becomes activated in response to extracellular stimuli through GEF-mediated GDP displacement followed by GTP binding, and then returns to its inactive state via GAP-mediated GTP hydrolysis. RAS is shown here in complex with the GEF SOS1 and with the GRD domain of the GAP NF1

(PDB structures 1XD2 and 6OB2, respectively). Mutations that prevent GAPs from assisting GTP hydrolysis halt the deactivation process and result in an accumulation of active, GTP-bound RAS. (Active RAS structure PDB:6VC8, inactive RAS structure PDB:6MBT)

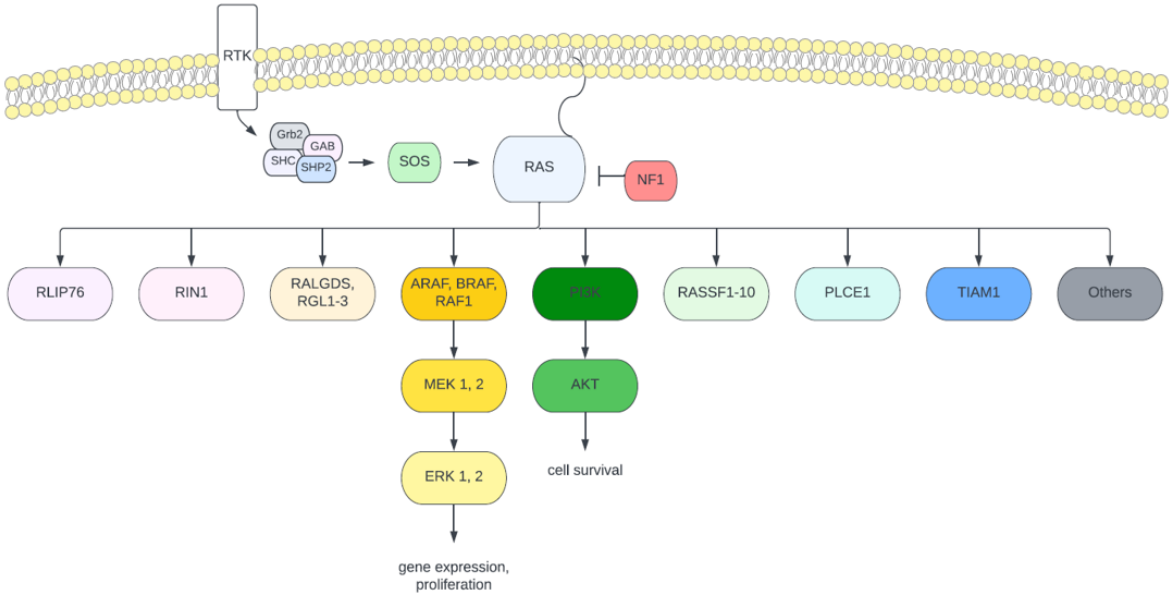

Figure 2. **RAS signaling pathways.** RAS proteins act as intermediary switches at the plasma membrane, interpreting extracellular signals via receptor tyrosine kinases (RTKs), which, when stimulated, trigger nucleotide exchange mediated by Guanine Exchange Factors (GEFs). The RAS GEF SOS1 is shown here. Once in its active GTP-bound state, RAS can potentiate several signaling cascades, including the MAPK (shown in yellow) and PI3K (shown in green) pathways, which are overactive in many cancers. Under normal signaling conditions, RAS is inactivated by GTPase activating proteins (GAPs), such as NF1, which catalyze GTP hydrolysis and return the protein to its inactive, GDP-bound state.

Interestingly, RAS isoforms play distinct biological roles despite sharing the same regulators and effectors. Mouse models lacking KRAS4b die during mid-gestation, while KRAS4a-, NRAS- and HRAS-null mice survive (Umanoff et al., 1995; Johnson et al., 1997; Koera et al., 1997; Esteban et al., 2001). However, replacement of KRAS with HRAS at the endogenous loci was shown to rescue development, despite causing dilated cardiomyopathy in adult mice, suggesting that RAS gene regulation may play a more

important role in development than isoform-specific signaling (Potenza et al., 2005). KRAS is also enriched with rare codons compared to HRAS and NRAS, and is generally expressed at lower relative levels (Pershing et al., 2015).

Differential protein processing, trafficking, and localization may account for some of the discrepancies in RAS isoform biological activity. The terminal -CAAX sequence (where A is an aliphatic amino acid and X is any amino acid) in the HVR of each isoform is the target of post-translational modification in the endoplasmic reticulum during initial protein processing (Hancock et al., 1989). The cysteine residue is modified with a farnesyl group on all RAS proteins by farnesyltransferases, which is essential for membrane localization (Hancock et al., 1989). Following this prenylation, RCE1 (RAS converting CAAX endopeptidase 1) cleaves -AAX residues, and the terminal cysteine is carboxymethylated by ICMT (isoprenylcysteine carboxyl methyltransferase) (Gutierrez et al., 1989). HRAS and NRAS are then trafficked through the Golgi, where DHHC9 and GCP16 add one palmitoyl group to NRAS and two to HRAS (Swarthout et al., 2005). This palmitoylation process is reversible, and is responsible for the continual shuttling of HRAS and NRAS between the plasma membrane and the Golgi (Rocks et al., 2005). KRAS4a is palmitoylated once by an unknown enzyme, and appears to localize to the plasma membrane without moving through the Golgi (Laude and Prior, 2008). KRAS4b is the only isoform that does not undergo palmitoylation, and instead engages the plasma membrane's negatively charged phospholipid head groups through electrostatic interactions with a string of six adjacent lysine residues in its HVR (Hancock et al., 1990). KRAS4b localization occurs independently of the secretory pathway, and is assisted by the GDI-like solubilizing factor PDEδ (Chandra et al., 2012).

Additional isoform-specific post-translational modifications have been detected on RAS that are hypothesized to affect its localization. For instance, KRAS generally localizes to and signals from the inner leaflet of the plasma membrane, but has been shown to relocate to endomembrane compartments of the mitochondria, Golgi and endoplasmic reticulum upon phosphorylation of serine 181 within the HVR by PKC, a process associated with Bcl-XL interaction and apoptosis (Bivona et al., 2006). The ubiquitination of HRAS and NRAS has been observed, and HRAS ubiquitination results in relocation to the endosome and reduced MAPK signaling potential (Jura et al., 2006).

RAS mutant frequencies in human cancers

Mutations that prevent GAP-mediated GTP hydrolysis increase the proportion of active, GTP-bound RAS and over-activate downstream signaling pathways. Somatic mutations in the RAS family occur the most frequently in human cancers, with roughly 19% of all tumors carrying driver mutations in one of the three human isoforms *KRAS, HRAS,* or *NRAS* (Prior et al., 2020). Mutations along the same pathways, such as the RAS regulators neurofibromin and SPRED1, upstream receptors, and downstream effectors BRAF and PIK3CA, also make a significant contribution to cancer (Simanshu et al., 2017). Germline mutations in *RAS* genes and their regulators cause a number of developmental disorders collectively known as "Rasopathies" (Simanshu et al., 2017). These *RAS* mutations are less aggressive than those found in cancers, with a lower proportion of the protein remaining in the active state. Over 400,000 individuals suffer from Rasopathies in the United States alone (Simanshu et al., 2017).

Cancer types show marked differences in RAS isoform mutational frequency; NRAS mutations drive 29% of melanomas, HRAS is primarily mutated in head and neck squamous cell carcinoma and bladder urothelial carcinoma, and KRAS mutations predominate in pancreatic ductal, lung, and colorectal adenocarcinoma (Moore et al., 2020). Of the three isoforms, KRAS is the most commonly found overall; 81% of RAS mutant tumor samples carry KRAS mutations, compared to 14% carrying NRAS and 5% HRAS (Figure 3). As such, KRAS has taken the brunt of the recent relentless drug discovery effort, with its more dominantly expressed KRAS4b splice variant gaining special attention. Precisely why KRAS is the main driver of so many cancers compared to its sister isoforms has been the subject of over four decades of research.

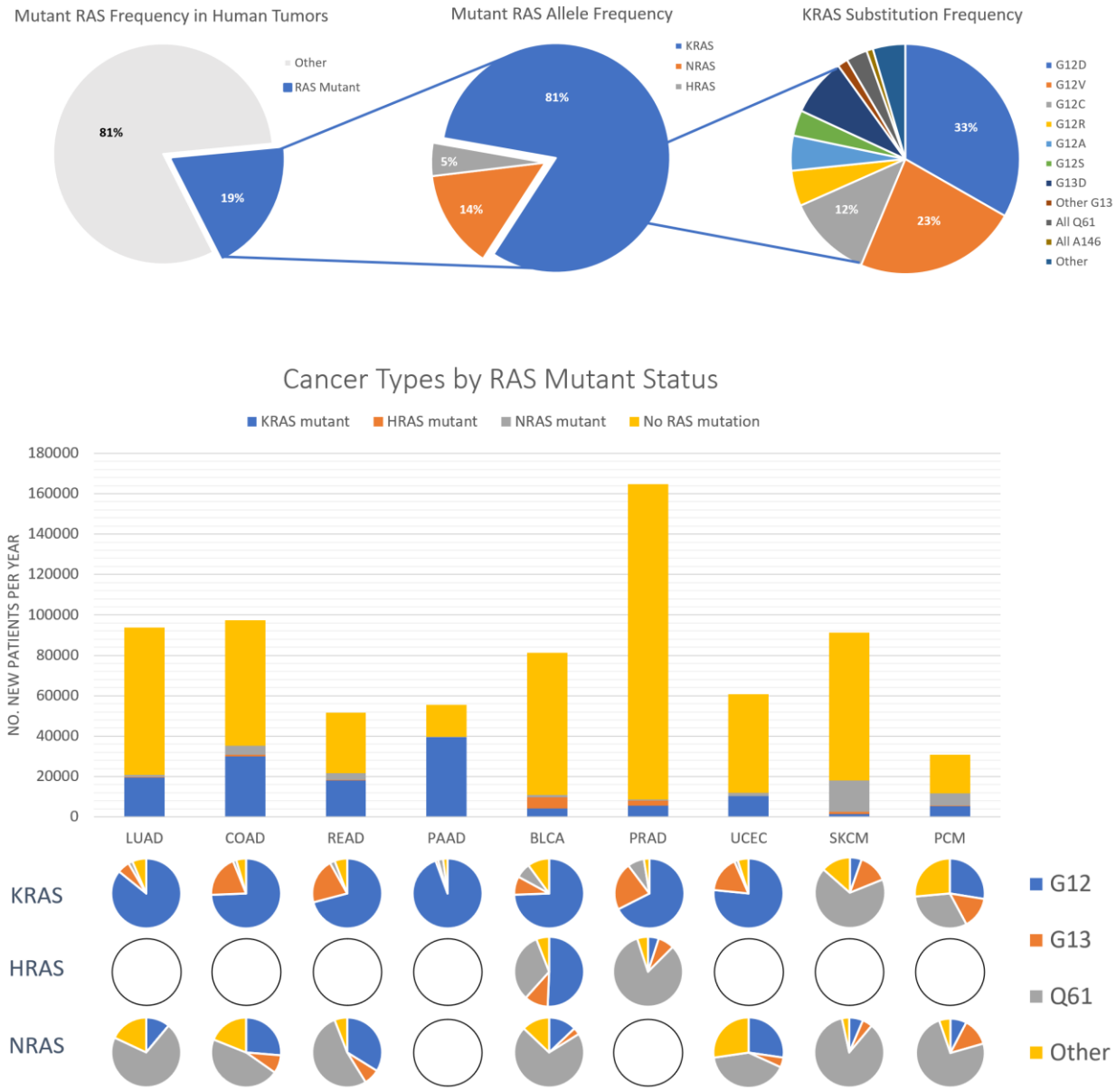

Figure 3. **RAS mutation frequencies in human cancers.** Frequency of RAS mutations identified in patient samples from the COSMIC, cBioPortal, ICGC, and TCGA databases (data sourced from Prior et al., 2020). Abbreviations: Lung adenocarcinoma (LUAD), colon adenocarcinoma (COAD), rectal adenocarcinoma (READ), pancreatic adenocarcinoma (PAAD), bladder urothelial carcinoma (BLCA), prostate adenocarcinoma (PRAD), uterine corpus endometrial carcinoma (UCEC), skin cutaneous melanoma (SKCM), plasma cell myeloma (PCM). Blank circles indicate insufficient data for quantification. Empty circles represent insufficient data.

Specific substitutions are also found heterogeneously across tissue types, which has similarly perplexed scientists. For instance, 80% of all oncogenic KRAS mutations occur at codon 12, but this accounts for 92% of KRAS mutations in PDAC versus 64% of KRAS mutations in colorectal cancer (Prior et al., 2012; Hobbs and Der, 2019). Of all G12 KRAS mutations across several datasets, aspartic acid substitutions occur most frequently (33%), followed by valine (23%) and cysteine (12%) (Figure 3) (Prior et al., 2012). Recent drug discovery efforts have focused on KRAS4b G12C due to its easy susceptibility to covalent attack, and several of these inhibitors have reached clinical trials (Liu et al., 2021). Discovery of an inhibitor targeting the less reactive aspartic acid substitution has proven more challenging; however, potent, selective, covalent and non-covalent inhibitors are currently in development (Wang et al., 2021; Zheng et al., 2022).

Some of these discrepancies in KRAS codon substitutions may be explained by mutagen exposure. There is evidence that tobacco smoke carcinogens, such as Benzo[a]pyrene diol epoxide (BPDE), are responsible for the predominance of G12C mutations in lung adenocarcinoma (Menzies et al., 2021). It is also notable that the most common KRAS mutations, G12D and G12V, occur through middle base substitutions (Prior et al., 2012). Mutagen exposure likely does not account for all known substitution frequencies, however. Current scientific consensus asserts that the majority of oncogenic mutations are caused by random replication errors (Tomasetti and Vogelstein, 2015). In agreement with this theory, a 2021 analysis of 13,492 patient samples concluded that known mutagenic mechanisms only partially explain the current spread of KRAS mutations, suggesting that biological selection likely also plays a role (Cook et al., 2021). The number of necessary base pair substitutions also contributes to mutant frequency; all

common oncogenic mutants only require a single base substitution. RAS mutations that are activating in vitro but require more than one substitution, such as G12I, G12L, and G12T, are predictably less common (Prior et al., 2012).

RAS structural characteristics

The secondary structure of RAS's G domain is typical of GTP-binding proteins, and contains five alpha helices surrounding a central beta-pleated sheet of six strands, five running parallel and one running antiparallel (Wittinghofer and Pal, 1991). Ten loops connect each helix or strand, six of which face the cytosol. Of these six, five loops are directly involved in nucleotide binding. Loop L1, also termed the 'phosphate-binding' or 'P-loop,' holds the negatively charged β and γ-phosphates of GTP in place with main chain hydrogens and a lysine. Mg^{2+} sits within this nucleotide-binding pocket, further neutralizing the phosphates and greatly increasing the affinity of RAS for either GDP or GTP (Wittinghofer and Pal, 1991).

Two regions surrounding the nucleotide are critical in defining the active vs inactive conformations, and are termed the switch I and switch II domains (residues 32-38 and 59-67, respectively) (Milburn et al., 1990; Vetter and Wittinghofer, 2001). When RAS is active and bound to GTP, switch I and switch II are ratcheted together by Thr35 in switch I and Gly60 in switch II, which form main chain hydrogen bonds with the gamma phosphate of GTP between them and hold RAS in a loaded spring conformation (Gasper and Wittinghofer, 2020). Once the gamma phosphate is hydrolyzed, these interactions are broken, and the spring is released. A comparison of many different RAS

structures revealed more flexibility in the switch regions of the inactive, GDP-bound structure when compared to the loaded, GTP-bound form (Vetter and Wittinghofer, 2001).

Both Thr35 and Gly60 are highly conserved within GTPase structures (Gasper and Wittinghofer, 2020). Mutational studies in which Thr35 is changed to Ser revealed more dynamic switch regions and a reduced affinity for effectors—a surprising change for such a conservative swap, and a clue that the methyl group is needed for switch I stabilization (Spoerner et al., 2001). An alanine substitution at glycine 60 significantly alters switch region conformation and reduces biological activity (Hwang et al., 1996; Ford et al., 2005). As such, these two residues are essential in coordinating switch region conformation and protein function.

NMR studies of RAS in complex with the non-hydrolyzable GTP analog GppNHp show two conformational states (Spoerner et al., 2001). State 1 is highly dynamic, and both T35S and T35A mutations were seen to exist exclusively in this state (Spoerner et al., 2001). Later crystal structures revealed a loss of main chain hydrogen bonds between both Thr35 and Gly60 and the GTP analog in this state (Muraoka et al., 2012). The more static second state maintains these bonds and shows RAS's conformation when in complex with effectors (Gasper and Wittinghofer, 2020).

The intrinsic GTPase activity of RAS proteins is markedly slow ($10^{-4}s^{-1}$), and relies on catalysis from GTPase activating proteins (GAPs) to shift to an inactive, GDP-bound form (Gasper and Wittinghofer, 2020). Mutational studies show a highly conserved arginine residue, or "arginine finger," within RAS GAP proteins as essential to complete this reaction (Ahmadian et al., 1997). In order to study this reaction, Scheffzek

et al. created a complex mimicking the transition state of this reaction between GDP-bound HRAS, the catalytic fragment of p120GAP (named GAP334), and aluminum fluoride (AlFx) (Scheffzek et al., 1997). The solved structure they generated revealed the GAP's arginine residue neutralizing negative charges arising in the transition state (Scheffzek et al., 1997). GAP334 was also shown to stabilize RAS's switch II region so that glycine 61 could maintain the nucleophilic water's position relative to the γ-phosphate and further aid in catalysis (Scheffzek et al., 1997). Any substitution at position 61 directly prevents intrinsic GTP hydrolysis and GAP activity by hindering this process. Mutations within the phosphoryl binding loop at glycine 12 or 13, however, sterically block the GAP arginine finger from neutralizing the transition state, and therefore maintain RAS in its active, GTP-bound form by preventing GAP-mediated hydrolysis.

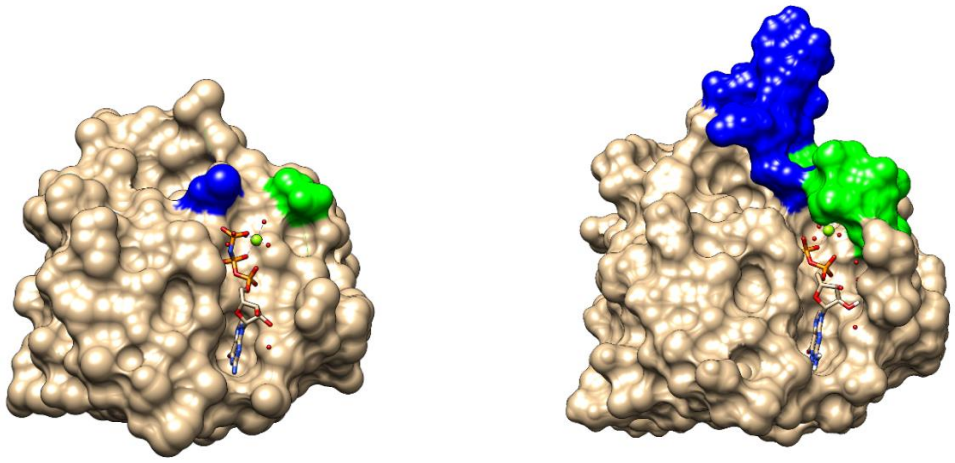

Figure 4. **Switch I and II regions in active and inactive RAS.** (**a**) Surface model (PDB:6VC8) of KRAS bound to GTP analog GppNHp with switch I residues (32-38) shown in green and switch II residues (59-67) in blue. A Mg^{2+} ion is also shown in green. (**b**) Surface model (PDB:6MBT) of KRAS bound to GDP with switch I residues shown in green and switch II residues shown in blue.

With rapid advancements in the field, we continue to learn more about differences in structure and conformation among RAS mutant proteins (Wittinghofer and Pal, 1991; Scheffzek et al., 1997). However, significant gaps in our knowledge remain; for instance, how exactly do common oncogenic substitutions alter RAS's conformation and movement, and how might these differences affect RAS biology and disease outcomes?

RAS mutants have distinct biochemical properties

Each mutant is reported to have unique biochemical properties distinct from wildtype RAS (Hunter et al., 2015). All oncogenic mutants have reduced intrinsic hydrolysis rates compared to the unmutated protein, but to varying extents (Hunter et al., 2015). Hunter et al. reported G12C proteins to have the fastest relative rate of intrinsic hydrolysis, over 2-fold higher than G12D, 5-fold higher than G13D, 10-fold higher than G12V, and roughly 50-fold higher than G12R, Q61H, G12A, and Q61L. Relative rates of GAP-stimulated GTP-hydrolysis showed less variation, with G12D having the fastest rate, roughly 3-fold higher than G12A, 4.5-fold higher than G12C, G12R, G12V, and G13D, 7-fold higher than Q61L, and 18-fold higher than Q61H.

RAS's hydrolysis rate is only one of three processes that influence the protein's predominant nucleotide state, however; GDP dissociation and GTP dissociation also contribute. If intrinsic hydrolysis occurs at the fastest rate, as it is in the wildtype protein, then the protein will exist mostly in its inactive, GDP-bound state. If GDP dissociation is fastest, then the protein will accumulate in the GTP-bound form and be hydrolyzed at a rate specific to each mutant (Burge and Hobbs, 2022). If both GTP and GDP dissociation

are fast and intrinsic hydrolysis is slow, the protein will exist predominately in its GTP-bound form (Burge and Hobbs, 2022). Each of these must be considered when predicting the relative activation states across mutant RAS proteins in cancers, along with differences in binding affinities for GAPs and GEFs, tissue-specific availability of GAPs, GEFs and receptors, cellular concentrations of GTP/GDP, receptor activation levels, and feedback signaling.

For instance, KRAS G13D (like all oncogenic mutants) has a reduced intrinsic hydrolysis rate, but an elevated GTP dissociation rate and a greater ability to be hydrolyzed by the GAP NF1, and so may exist in GDP-bound and nucleotide free states for longer than other mutants (Rabara et al., 2019; Burge and Hobbs, 2022). Consequently, KRAS G13D mutations are often coupled with inactivating mutations in *NF1* in human cancers (Rabara et al., 2019). KRAS G12D has a higher GTP dissociation rate than the wildtype protein, so while it exists primarily as GTP-bound, there may be a subpopulation of nucleotide free KRAS G12D (Burge and Hobbs, 2022). KRAS Q61R is virtually incapable of intrinsic hydrolysis and also has a low GTP dissociation rate, and so exists almost exclusively in its GTP-bound state (Burge and Hobbs, 2022).

It is important to note that predicted nucleotide state does not directly translate to tumorigenic potential or frequency of occurrence in human cancers. For instance, KRAS Q61R likely exists in the highest proportion of GTP-bound protein, yet is mutated at a much lower frequency than KRAS G12D, G12C, or G12V. One theory proposes that mutations must hit a “sweet spot” of signaling to induce tumorigenesis—too much triggers abortive processes like apoptosis, and too little fails to drive enough cell division to cause cancer (Li et al., 2018). This is supported by a Pershing et al.’s 2014 study,

which found that mice with one allele of KRAS mutated to replace rare codons with common codons (and therefore driving higher KRAS expression) were more resistant to urethane exposure than mice with wildtype alleles (Pershing et al., 2015). In this study, mutant forms of KRAS expressed at higher levels induced growth arrest. When the KRAS allele with common codons was found to be oncogenic, only G12D mutations were detected, suggesting that strongly activating mutations are not tolerated at higher expression levels (Pershing et al., 2015). Given that HRAS and NRAS encode more common codons and are often expressed at higher levels, this may also explain the variation in substitution frequencies between alleles.

Phenotypic differences across RAS mutants

The question of whether differential structural and biochemical characteristics of RAS mutants affect their biological activity has long been investigated. Early experiments sought to uncover any meaningful differences between RAS mutant alleles in their oncogenic potential *in vivo*. A 1984 study revealed a range of transformation potentials across 20 HRAS codon 12 mutations when transfected into Rat fibroblasts (Seeburg et al., 1984). G12V, G12L, G12I, G12R, and G12T proteins exhibited the strongest transformation potential, with colonies growing rapidly and to the highest saturation densities (Seeburg et al., 1984). G12S, G12M, G12C, G12Y, G12F, G12W, G12H, G12D, G12E, G12A, and G12N showed intermediate potential, while G12K and G12Q mutations showed low transformation ability. A proline substitution at codon 12 failed to transform fibroblasts, likely due to significant structural changes induced by this mutation. Later experiments investigating codon 61 also found varying abilities of 17

mutants to form foci when transfected into NIH3T3 cells (Der et al., 1986). Q61V, Q61L, Q61K, Q61A, Q61C, and Q61R showed strong ability, Q61H, Q61I, Q61Y, Q61M, Q61T, Q61N, Q61W, and Q61F mutants showed intermediate, and Q61G showed very weak transformation potential (Der et al., 1986). Q61P and wildtype failed to form foci, and acted similarly to the wildtype protein (Der et al., 1986). Another early 1984 study subjected wildtype HRAS to random mutagenesis, and found HRAS G12V to be the most potent in focus formation ability, followed by G12R, G12D, G12S, and G13D in that order (Fasano et al., 1984).

Differential effector activation across RAS mutants

Subtle differences in mutant structures may alter RAS's ability to engage with specific effectors, which would help explain varying substitution frequencies across cancer types and phenotypic differences between RAS mutants. However, a comprehensive analysis of effector preferences across RAS mutant proteins has not been done, and existing studies report conflicting results.

RAS effector proteins selectively bind to GTP-loaded RAS via a conserved region containing a ubiquitin-like fold, termed the RAS binding domain (RBD) (Burge and Hobbs, 2022). Although all have similar topology, these domains fall into three distinct classes: RAS-associated domains (RAs), RAS binding domains (RBDs), and PI3K RAS binding domains (PI3K RBDs) (Kiel et al., 2021). The human genome is predicted to have 56 proteins containing an RBD, spanning 12 signaling pathways (Kiel et al., 2021).

17 of these proteins are known to bind directly to RAS, measured in vitro through biophysical techniques, 8 of which are high affinity binders (Kiel et al., 2021).

RAF1 kinase was the first RAS effector to be discovered, and has since been shown to have the highest affinity for RAS of all known effectors (Morrison et al., 1988; Burge and Hobbs, 2022). RAF1 activates the MAP kinase pathway, which is a strong driver of cellular proliferation and is the most consequential signaling pathway to RAS-driven cancers (Burge and Hobbs, 2022). RAF1 is one of three members of the RAF serine/threonine kinase family known to bind directly to RAS and initiate MAPK signaling; ARAF and BRAF are also ubiquitously expressed and play key roles in this signaling pathway. All RAF kinases are maintained in an autoinhibited, cytosolic state in complex with 14-3-3 and HsP90 before undergoing a complex process of activation (Terrell and Morrison, 2019). The sequence of events in RAF recruitment, release of autoinhibition, and activation is still debated; however, binding of the RBD to GTP-bound RAS is an essential step, and is believed to initiate the process by localizing RAF to the membrane (Terrell and Morrison, 2019). A cysteine-rich domain (CRD) adjacent to the RBD also assists in membrane localization, likely through electrostatic interactions with phosphatidylserine lipid head groups within the membrane (Bondeva et al., 2002; Terrell and Morrison, 2019). Recent crystal structures revealed that both the RBD and CRD regions of RAF1 interact extensively with KRAS, and mutations at the CRD-KRAS interface reduced RAF1 activation in cells (Tran et al., 2021). Additionally, over 40% of activating BRAF mutations found in the RASopathy Cardiofaciocutaneous syndrome (CFC) occur within the CRD, further supporting its role in recruitment and activation (Sarkozy et al., 2009). Following RBD-CRD binding, 14-3-3 is displaced from the n-

terminal CR2 region while maintaining contact at the c-terminal tail (Terrell and Morrison, 2019). This allows for the serine/threonine-rich CR2 region to become dephosphorylated by a complex of MRAS, SHOC2, and PP1 (Rodriguez-Viciana et al., 2006). The n-terminal regions of ARAF and RAF1 are then phosphorylated, which is necessary for the release of autoinhibition and subsequent activation. BRAF maintains a negative charge at its n-terminus with two aspartic acid residues and a constitutively phosphorylated serine site (Ritt et al., 2007). RAF proteins then homo- or heterodimerize, which is necessary for signal potentiation under most circumstances (Rodriguez-Viciana et al., 2006).

Cellular, biochemical, and tumor studies into RAF-RAS mutant binding affinity and downstream activation have reached varying conclusions. Predictably, reported values of RAS affinity are much higher for RAF RBD than full-length RAF, as the truncated region lacks autoinhibitory domains and binding sites for regulatory proteins. Early experiments found KRAS4b G12V to be superior to KRAS4a G12V, NRAS G12V, and HRAS G12V (in that order) in activating RAF1 in COS-1 cells (Voice et al., 1999). In 2008, Rosseland et al. reported that overexpression of HRAS G12V but not KRAS G12V potentiated EGF-induced proliferation in primary hepatocytes (Rosseland et al., 2008). In support of this finding, Stolze et al. found isogenic MCF10A cell lines expressing KRAS G12D, G12V, and G13D to induce EGF-independent proliferation whereas KRAS WT-, G12C-, and G13C-expressing cell lines did not (Stolze et al., 2015).

Cespedes et al. found that KRAS G12V conferred significantly greater oncogenic potential to NIH3T3 cells in a mouse xenograft model when compared to KRAS G12D (Céspedes et al., 2006). In this model, KRAS G12V mutant tumors proliferated seven

times faster, interacted with RAF1, and induced higher levels of phosphor-ERK when compared to G12D, which was not found to interact with RAF1 as measured by RBD pull-downs of tumor lysates (Céspedes et al., 2006). Interestingly, KRAS G12C-mutant cells were unable to induce tumorigenesis (Céspedes et al., 2006). In contrast, Haigis et al. found KRAS G12D expression in the colonic epithelium of mice induced MEK-dependent hyperproliferation, raising the importance of tissue context-dependent differences in KRAS-mutant outcomes (Haigis et al., 2008). In 2015, Hunter et al. reported a marginal decrease in affinity for RAF1-RBD by G12C, and a significant decrease in affinity by G12D when compared to the wildtype protein as measured by a proximity-based luminescence competition assay (Hunter et al., 2015). However, purely biochemical measurements of the RBD alone should be interpreted cautiously, as they do not account for interactions with the CRD, membrane, and regulatory proteins present in a cellular environment.

Phosphatidylinositol 3-kinases (PI3Ks) are heterodimeric lipid kinases that regulate cellular processes such as transformation, growth, adhesion, survival, apoptosis, vesicle trafficking, metabolism, and motility (Fruman et al., 1998). PI3Ks are composed of regulatory and catalytic subunits, which are encoded for by separate genes (Castellano and Downward, 2011). The Class I PI3K family is the best characterized and most widely implicated in cancer. Class I catalytic subunits p110α, p110β, p110γ, and p110δ are encoded for by *PIK3CA, PIK3CB, PIK3CG,* and *PIK3CD* genes, respectively (Castellano and Downward, 2011). Subunits p110α, p110β, and p110δ bind the p85 type regulatory subunit, while p110γ binds either the p101 or p87 regulatory subunits. Gain-of-function mutations occur frequently in PIK3CA, and stimulate AKT signaling, induce anchorage-

independent growth in culture, and cause tumor growth in vivo (Isakoff et al., 2005; Samuels et al., 2005; Bader et al., 2006; Gymnopoulos et al., 2007). PIK3CA mutations are commonly found in glioblastomas, gastric cancers, breast cancers, and lung cancers (Samuels et al., 2004).

Activated PI3Ks convert lipids phosphatidylinositol (4,5)- bisphosphate (PI(4,5)P2) and phosphatidylinositol (4)-phosphate (PI(4)P) to phosphatidylinositol (3,4,5)-trisphosphate (PIP3) and phosphatidylinositol (3,4)-bisphosphate (PI(3,4)P2), respectively (Castellano and Downward, 2011). The accumulation of PIP3 second messenger lipids recruits phosphoinositide-dependent kinases PDK1 and PDK2, which then phosphorylate and activate AKT. Propagation of these pathways by PI3Ks has been shown to be essential for both tumor initiation and maintenance (Lim and Counter, 2005).

PI3Ks are activated by three known mechanisms, all involving receptor tyrosine kinase stimulation and translocation to the inner leaflet of the plasma membrane (Castellano and Downward, 2011). Direct engagement of GTP-bound RAS by the PI3K RBD of the p110 catalytic subunit is one method of activation (Castellano and Downward, 2011; Simanshu et al., 2017). PI3Ks are regarded as critical RAS effectors, although they bind to RAS with a much lower affinity than RAF kinases (Pacold et al., 2000). The propagation of PI3K-driven signaling pathways appears to be necessary for cancer, but the dependence of PI3Ks on RAS for activation is likely tissue-specific (Burge and Hobbs, 2022). For instance, RAS and PI3K pathway mutations are mutually exclusive in breast cancers, but PIK3CA and RAS mutations often co-occur in colorectal and endometrial cancers (Castellano and Downward, 2011). KRAS G12R mutant proteins cannot bind to p110α due to structural alterations in the switch II region (Hobbs

et al., 2020). G12R mutations constitute roughly 1% of lung and colorectal cancers, but occur in 20% of pancreatic ductal adenocarcinomas (PDAC) (Hobbs et al., 2020); however, this subset of PDAC tumors is associated with a higher incidence of PI3K pathway mutations, providing further evidence of the need for this pathway in cancer (Diehl et al., 2021).

Specific differences in PI3K engagement across other mutants has not been widely studied. A comparison of isogenic MCF10A (breast epithelial) cell lines driven by KRAS G12C, G12D, G12V, G13C, G13D, A18D, Q61H, and K117N mutations showed no differences in basal or EGF-stimulated AKT activation (Stolze et al., 2015). However, a comparison by Ilhe et al. of NSCLC cell lines showed activated PI3K and MAPK signaling in cell lines carrying KRAS G12D mutations, while KRAS G12C- or G12V-mutant lines showed decreased growth factor-dependent AKT activation, again raising the importance of cell-type-specific patterns of effector engagement (Ihle et al., 2012).

Several transgenic murine tumorigenesis models have also shown mutant-specific differences in PI3K signaling. Cespedes et al. reported that nude mouse xenografts from KRAS G12D-mutant NIH3T3 fibroblasts transduced signals exclusively through the PI3K/AKT pathway when compared to G12C or G12V models (Céspedes et al., 2006). G12V xenografts grew at a more aggressive rate and interacted with both RAF1 and PI3K, while G12C xenografts failed to form tumors (Céspedes et al., 2006). In another study, mice carrying KRAS G12D mutations and RBD-deficient p110α mutations failed to drive carcinogenesis (Gupta et al., 2007).

A milder phenotype for KRAS G12C-mutant cancers was also observed in an *in utero* exposure model, where mice were subjected to 3-methylcholanthrene and observed

for tumor formation (Leone-Kabler et al., 1997; Gressani et al., 1999; Jennings-Gee et al., 2006). Mice that obtained KRAS G12V, G12D, G12R, and G13R mutations were significantly more likely to develop later-stage tumors six to twelve months after birth than mice with KRAS G12C or no KRAS mutation at all (Leone-Kabler et al., 1997; Gressani et al., 1999; Jennings-Gee et al., 2006). Similarly, tetracycline-inducible, lung-specific murine tumorigenesis models showed KRAS G12C expression in mice induced multiple small lung tumors over twelve months, a less aggressive outcome than seen in similar systems expressing KRAS G12D or G12V mutant alleles (Fisher et al., 2001; Jackson et al., 2001; Johnson et al., 2001; Meuwissen et al., 2001; Floyd et al., 2005). This G12C system did show increased MAPK activation measured by ERK phosphorylation, but did not show an increase in AKT signaling (Floyd et al., 2005).

Differences in RAS mutant structure and biochemical properties have been instrumental in the search for targeted therapeutics, which has reached a golden age with the recent discovery of G12D-, G12S-, and G12R-specific drugs (Christensen, 2021; Zhang et al., 2022a; Zhang et al., 2022b). Certain differences in RAS mutant biochemical properties have also informed our understanding of how to target select pathways. For instance, KRAS G13D-GTP was shown to be hydrolyzed by NF1 GAP, rendering KRAS G13D-mutant cells sensitive to EGFR inhibitors in an NF1 wildtype context (Rabara et al., 2019). Also, the discovery that KRAS G12R is incapable of interacting with p110α may imply that AKT pathway inhibitors would be beneficial for patients with this mutation (Hobbs et al., 2020).

Despite great advancements in our understanding of RAS's structural and biochemical characteristics, there are significant gaps in our understanding of how RAS

mutants engage effectors and interactor proteins; the data are contradictory and incomplete. Such knowledge would be valuable to the pursuit of targeted therapeutics, and could inform the choice of combination therapies and improve patient outcomes. In this thesis, we evaluate the binding preferences between common oncogenic mutants KRAS4b G12D and KRAS4b G12C and their effectors RAF1 and p110α using quantitative, cellular-based techniques.

Bioluminescence Resonance Energy Transfer (BRET)

Bioluminescence Resonance Energy Transfer (BRET) is a powerful tool for studying protein-protein interactions. The naturally occurring phenomenon was initially found in sea creatures such as the sea pansy *Renilla reniformis* and jellyfish *Aequorea Victoria*, which are proposed to use the luminescent glow to ward off predators, and was later adopted by scientists in the explosion of bioluminescence-based molecular techniques. The process involves the dipole-dipole transfer of energy from an enzymatic donor to a fluorescent acceptor protein (Pfleger and Eidne, 2006). In contrast to its sister technique Fluorescence Resonance Energy Transfer (FRET), which requires the excitation of a donor fluorophore, the BRET reaction is initiated by a donor enzyme oxidizing its substrate. In this way, BRET avoids certain technical drawbacks of FRET such as photobleaching, autofluorescence, and direct excitation of the acceptor (Weihs et al., 2020). However, it requires the fusion of either an acceptor or donor protein tag to the protein of interest, which may impede its structure and function.

The efficiency of energy transfer between two chromophores depends on the inverse sixth-distance between them (Weihs et al., 2020). The Förster distance (R0) is the distance at which half of the energy is transferred from donor to acceptor, and is a function of several factors, including the quantum yield of the donor, the refractive index of the solution, the spectral overlap between donor emission and acceptor excitation, the relative orientation between the chromophores' transition dipole moments, and their physical separation (Weihs et al., 2020). Protein-protein interaction studies may benefit from a smaller Förster distance to minimize detection of non-specific interaction, which is particularly important for investigating interactions within a cellular membrane (Weihs et al., 2020).

Here, we utilize the 19kDa luciferase NanoLuc, engineered from a luciferase subunit found in the deep sea shrimp *Oplophorus gracilirostris* as the donor enzyme (Hall et al., 2012). With its substrate furimazine, the specific activity of NanoLuc is ~150-fold greater than previous generation *Renilla* or firefly luciferases (Hall et al., 2012). This superior brightness allows for detection of low, endogenous levels of expression (Hall et al., 2012). When paired with the monomeric Venus variant mVenus, resonance energy transfer occurs with a Förster distance (R0) of 5.59nm, and is detected at an emission peak of 530nm (Figure 5) (Kremers et al., 2006; Weihs et al., 2020).

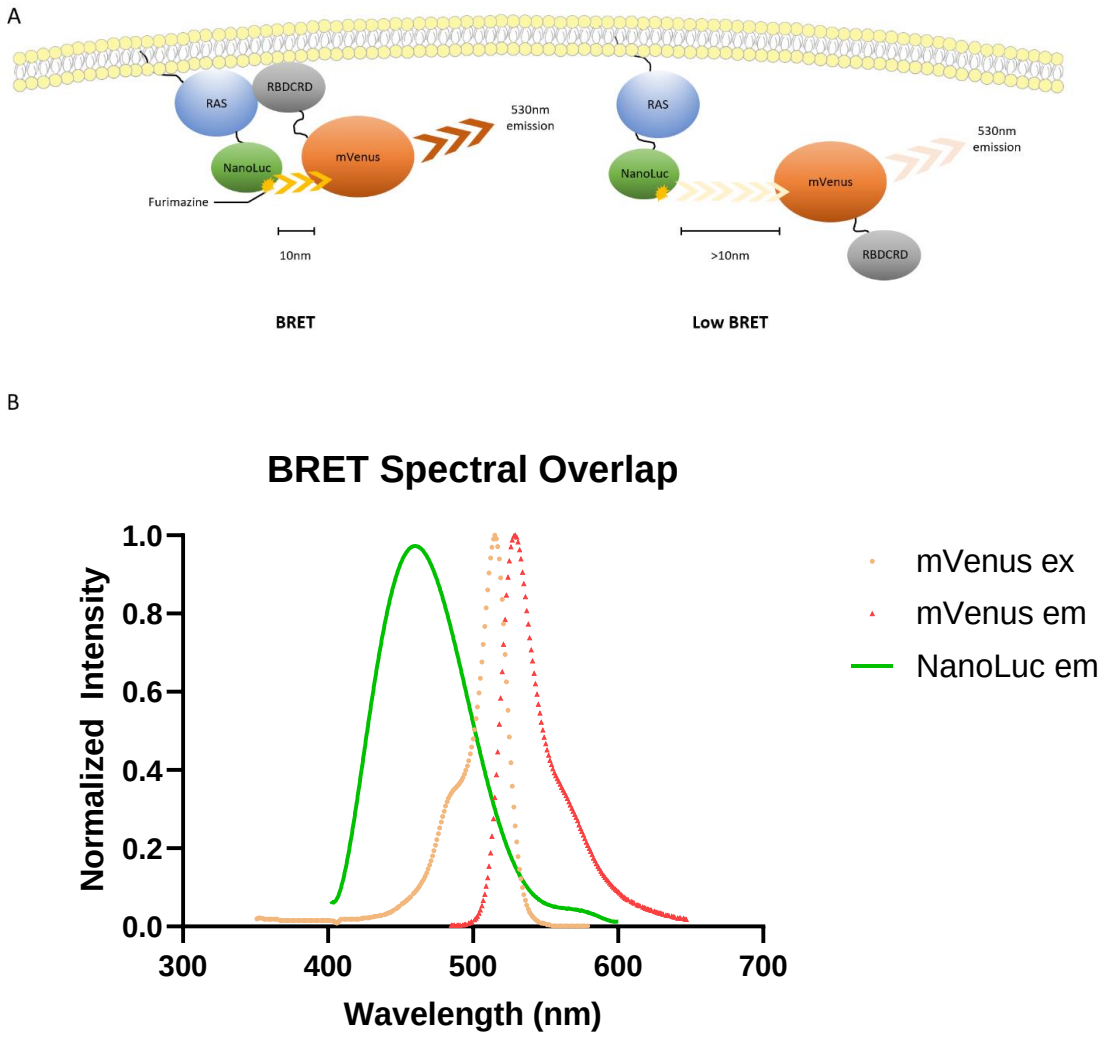

Figure 5. **BRET interactions and spectral overlap.** (**a**) Bioluminescence Resonance Energy Transfer between RAF1(52-188)-NanoLuc and mVenus-RAS proteins(Mo and Fu, 2016). Addition of the NanoLuc substrate furimazine initiates resonance energy transfer with mVenus molecules with a high efficiency within a 10nm radius. BRET efficiency is significantly lower at distances above 10nm (**b**) Spectral overlap between NanoLuc emissions, mVenus excitation, and mVenus emissions spectra. NanoLuc emissions peak at 460nm, mVenus excitation peaks at 515nm, and mVenus emissions peak at 530nm.

Detection and quantitation of specific, live-cell protein-protein interactions can be achieved through BRET saturation experiments (Mercier et al., 2002; Terrillon et al., 2003; Ayoub et al., 2004; Breit et al., 2004; Wilson et al., 2005; Pfleger and Eidne,

2006). In this technique, levels of donor expression are kept low and constant while acceptor expression is systematically increased. When BRET signal is plotted against Acceptor/Donor expression values, data from a non-specific interaction will rise in a quasi-linear fashion, while specific interactions increase sharply and then level off as all possible donor-acceptor protein pairs are achieved (Pfleger and Eidne, 2006) (Figure 6). The measurements $BRET_{max}$ and $BRET_{50}$ can be extrapolated from a hyperbolic curve fit. $BRET_{max}$ values represent the maximum signal possible in the system, and the Acceptor/Donor ratio that produces half of the $BRET_{max}$ signal is interpreted as the $BRET_{50}$ value. $BRET_{50}$ values are a measurement of relative affinity. $BRET_{max}$ values are a function of tag orientation and maximum allowable occupancy between the protein pair of interest.

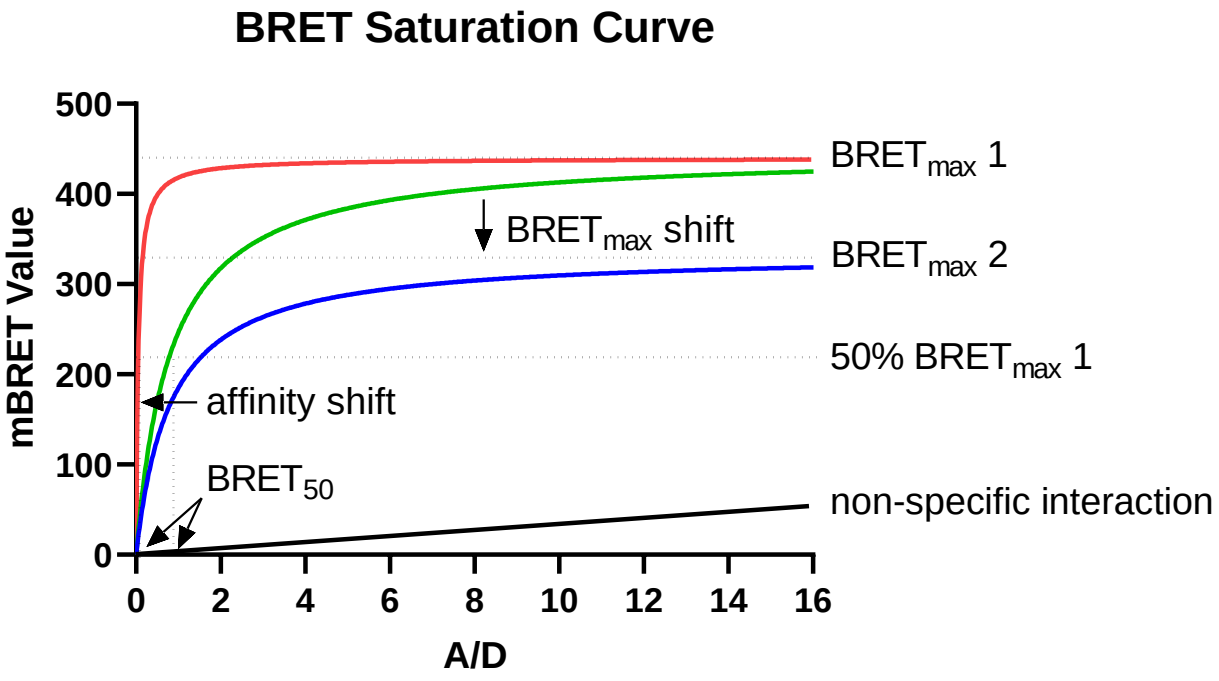

Figure 6. **Theoretical BRET saturation curves.** Specific protein-protein interactions when measured by BRET will saturate as acceptor concentrations increase and donor concentrations are maintained. The acceptor/donor value at 50% of the maximum signal

is reported as the $BRET_{50}$ value. In protein pairs with a higher affinity, this value will shift lower (shown here as green to red). Non-specific interactions will increase in a quasi-linear fashion. $BRET_{max}$ values are interpreted as the maximum signal attainable between the two proteins within the system. $BRET_{max}$ values are a function of relative occupancy and of tag orientation, which can affect BRET efficiency.

Here, we utilize Bioluminescence Resonance Energy Transfer (BRET) within a cellular system to characterize engagement of effectors RAF1 and p110α by KRAS4b G12D, KRAS4b G12C, and KRAS4b WT proteins. We also investigate endogenous effector engagement by performing pull-downs on Hela cell lines engineered to express KRAS mutants under the control of a doxycycline-inducible promoter.

RATIONALE

RAS mutations drive a substantial portion of human cancers, and have been the target of an extensive therapeutic search for decades. Substitutions in position 12, 13, or 61 maintain RAS in the active, GTP-bound state, and drive downstream signaling and oncogenesis. RAS mutational profiles differ significantly across cancer types, but the underlying cause for these discrepancies is not yet understood. KRAS4b G12C and G12D mutations are among the most common mutations in pancreatic, colorectal, and lung adenocarcinomas, which have particularly poor prognoses (Prior et al., 2012). Promising inhibitors specific for KRAS G12C have reached the clinic, and KRAS G12D inhibitors are not too far behind. However, it is still not clear if there are any differences in effector engagement and signaling behavior between these two mutants. Here, we interrogate the more highly expressed KRAS4b variant, and provide live cell

measurements of effector engagement between KRAS4b G12D, KRAS4b G12C, and KRAS4b wildtype and the effectors RAF1 and p110α as measured by Bioluminescence Resonance Energy Transfer (BRET). We also investigate relative endogenous effector engagement through pull-downs of tagged KRAS4b G12D and KRAS4b G12C in doxycycline-inducible HeLa cell lines, and transiently transfected HEK293T cells.

MATERIALS AND METHODS

Plasmid Construct Generation

Plasmid fusion constructs were generated using the combinatorial Multisite Gateway cloning system (Wall et al., 2014). A strong CMV51 promoter was combined with standard Gateway Entry clones encoding either NanoLuc or mVenus and various RAS or RAS effector constructs, with disordered linker sequences connecting the two regions (see Table 1). A generic mammalian expression Gateway Destination vector was used in all reactions. Synthetic templates were ordered from ATUM and cloned using a BP Gateway reaction into pDonr-255 to generate entry clones.

Clone ID	Fluorescent Tag	Clone Information	Entry Clone 1	Entry Clone 2	Entry Clone 3	Vector
R705-M40-304	mVenus	mVenus-Hs.KRAS4b (G12D)	CMV51 (Addgene 162973)	mVenus (Addgene 162943)	Hs.KRAS4b G12D (Addgene 38131)	pDest-304
R714-M09-304	mVenus	mVenus-Hs.KRAS4b G12C	CMV51 (Addgene 162973)	mVenus (Addgene 162943)	Hs.KRAS4b G12C (Addgene 83130)	pDest-304
R718-M86-305	mVenus	mVenus-Hs.KRAS4b	CMV51 (Addgene 162973)	mVenus (Addgene 162943)	Hs.KRAS4b (Addgene 83129)	pDest-305
R783-M26-303	mVenus	mVenus-PIK3CA	CMV51 (Addgene 162973)	mVenus (Addgene 162943)	Hs.PIK3CA (Addgene 70447)	pDest-303
R783-M27-313	mVenus	PIK3CA-mVenus	CMV51 (Addgene 162973)	Hs.PIK3CA (Addgene 70448)	mVenus (Addgene 162905)	pDest-313
R735-M41-303	mVenus	mVenus-Hs.RAF1(52-188)	CMV51 (Addgene 162973)	mVenus (Addgene 162943)	Synthetic template	pDest-303
R735-M42-313	mVenus	Hs.RAF1(52-188)-mVenus	CMV51 (Addgene 162927)	Synthetic template	mVenus (Addgene 162905)	pDest-313
R707-M08-304	mVenus	mVenus-Hs.RAF1	CMV51 (Addgene 162973)	mVenus (Addgene 162943)	Hs.RAF1 (Addgene 70497)	pDest-304
R735-M40-313	mVenus	Hs.RAF1-mVenus	CMV51 (Addgene 162927)	Hs.RAF1 (Addgene 70498)	mVenus (Addgene 162905)	pDest-313
R713-M62-305	NanoLuc	NanoLuc-PIK3CA	CMV51 (Addgene 162973)	NanoLuc (Addgene 162938)	Hs.PIK3CA (Addgene 70447)	pDest-305
R713-M65-312	NanoLuc	PIK3CA-NanoLuc	CMV51 (Addgene 162927)	Hs.PIK3CA (Addgene 70448)	NanoLuc (Addgene 162901)	pDest-312
R735-M43-303	NanoLuc	NanoLuc-Hs.RAF1(52-188)	CMV51 (Addgene 162973)	NanoLuc (Addgene 162938)	Synthetic template	pDest-303
R735-M44-313	NanoLuc	Hs.RAF1(52-188)-NanoLuc	CMV51 (Addgene 162927)	Synthetic template	NanoLuc (Addgene 162901)	pDest-313
R718-M11-303	NanoLuc	NanoLuc-Hs.RAF1	CMV51 (Addgene 162973)	NanoLuc (Addgene 162938)	Hs.RAF1 (Addgene 70497)	pDest-303
R718-M15-313	NanoLuc	Hs.RAF1-NanoLuc	CMV51 (Addgene 162927)	Hs.RAF1 (Addgene 70498)	NanoLuc (Addgene 162901)	pDest-313
R733-M02-305	NanoLuc	nL-KRAS G12D	CMV51 (Addgene 162973)	NanoLuc (Addgene 162938)	Hs.KRAS4b G12D (Addgene 38131)	pDest-305
R785-M04-303	none	empty vector	CMV51 (Addgene 162927)	stuffer (Addgene 162900)		pDest-303

Table 1. Plasmid DNA clone information. Plasmid DNA clones used, with clone ID, entry clone, and vector information. The above plasmid fusion constructs were generated using Multisite Gateway cloning.

Cell Culture

HEK293T cells (ATCC, CRL-3216) were cultured in complete phenol red free DMEM (Life Technologies, 31053-028, 4.5g/L Glucose, 3.7g/L Sodium Bicarbonate), 2mM L-Glutamine (Life Technologies, 25030081), and 10% tetracycline-free FBS (Takara Bio, 631101) at 37°C and 5% CO2.

HeLa cell lines were maintained in DMEM (Quality Biological, 112-014-101) fortified with 10% tetracycline-free FBS (Takara Bio, 631101). Cell lines were cultured under selection in concentrations of 4µg/mL blasticidin and 1µg/mL puromycin.

Cell Line Generation

HeLa cells (ATCC, CCL-2) were transduced at MOI 0.05 with lentivirus containing a CMV13p promoter and Tet regulated promoter TRE3G (plasmid construct R980-M38-658). Cells were incubated for 24 hours, after which complete media (described above) was removed and replaced. After an additional 24 hours, media was removed and replaced with complete media containing 4µg/mL Blasticidin. Cells were cultured for two weeks under selection before being aliquoted and frozen in vapor phase liquid nitrogen. HeLas were then regrown in culture and transduced with lentivirus containing a plasmid construct encoding a TRE3Gp promoter and meGFP-Hs.KRAS4b G12D at MOI 0.05 (R703-M53-663), meGFP-Hs.KRAS4b G12C at MOI1 (R733-M42-663), or meGFP-Hs.KRAS4b at MOI1 (R703-M52-663). New cell lines were cultured for an additional two weeks under selection with 4µg/mL Blasticidin and 1µg/mL Puromycin. All plasmids and virus were generated at the RAS Initiative.

BRET Saturation Curves

HEK293T cells were seeded at $1.4e^5$ cells per well of a 12-well plate in 1mL complete phenol red free DMEM in 10% FBS, and left to incubate at 37°C and 5% CO2 for 24 hours. Fugene 6 (Promega, E2691) was diluted into FBS-free phenol red free DMEM media and incubated at room temperature for 5 minutes. A 1:8 ratio of µg DNA to µL Fugene 6 was used for all transfected points. Plasmid DNA constructs were diluted in FBS-free DMEM media, combined with Fugene-DMEM mix, and incubated at room temperature for 15 minutes before being gently pipetted onto cells. Total µg DNA was kept constant across transfected points with empty plasmid. Cells were left to proliferate for an additional 24 hours. 0.6µg DNA was used as the top RAS construct concentration for RAF1(52-188) curves, and 1.8µg was used for PIK3CA comparisons.

Media was then aspirated, and 250µL of 0.05% trypsin was added for 3 minutes to lift cells into suspension. 750µL complete media was then added, and cells were transferred to 1.5mL microcentrifuge tubes, where they were gently pelleted by centrifugation and resuspended in 120µL 0.5% FBS dPBS. A volume of 120µL was chosen so that the lowest levels of mVenus-tagged KRAS4b G12D expressed in saturation curve points would still be detectable by the instrument. 20µL of each condition was then immediately pipetted into duplicate wells of both a white 384 well plate, and a black 384 well plate. 20µL of the NanoLuc substrate Furimazine (Promega, N1663) was added to the white plate for a final concentration of 10µM, and plates were shaken for 30 seconds on a plate shaker. After an incubation of exactly 10 minutes, emissions were measured on a Perkin-Elmer Envision plate reader using a 460/80nm

band-pass filter (NanoLuc donor signal) and a 530nm long-pass filter (BRET signal). 20µL 0.5% FBS dPBS was added to each well of the black 384-well plate, which was shaken on a plate shaker for 30 seconds and then excited at 500nm and read at 530nm (raw mVenus signal). Cells were not kept in suspension for longer than 1 hour to minimize stress and signaling changes associated with serum starvation.

BRET Curve Analysis

BRET ratios were defined by 530nm emissions signal (BRET) divided by the 460nm emissions signal (NanoLuc) of the unexcited sample (white plate). Background BRET ratios were taken from samples that were transfected with only donor DNA. One background sample was transfected per curve. MilliBRET values were then calculated with the following formula:

1000 x [(sample BRET ratio)-(avg background BRET ratio)]

mVenus expression was measured separately by excitation at 500nm and emission at 530nm in technical duplicates from the black plate. mVenus values for each transfected well were averaged and divided by NanoLuc emissions values from individual technical replicates to yield acceptor/donor values for each mBRET value. Corrected acceptor/donor (A/D) ratios were then determined using the following formula, where all points were normalized to a set internal curve point:

Raw A/D =

$$\frac{\textit{(sample A/D) – (avg background A/D)}}{\textit{(7}^{th}\textit{ point A/D from curve 1) – (avg background A/D)}}$$

Points were plotted using GraphPad Prism, and data were fit to a nonlinear regression hyperbolic curve model. $BRET_{max}$ and $BRET_{50}$ values were extrapolated from the curve fit. Statistical differences in $BRET_{max}$ and $BRET_{50}$ values were determined by a two-tailed paired t-test assuming unequal variance using Microsoft Excel.

Active RAS Pull-down

HeLa cell lines RPZ26802 (TetON eGFP-KRAS4b WT), RPZ26636 (TetON eGFP-KRAS4b G12D), and RPZ26942 (TetON eGFP-KRAS4b G12C) were seeded at 1e6 in 10mL media + doxycycline into 100mm dishes. Concentrations of doxycycline necessary to normalize expression across cell lines were previously determined by saturation experiments via flow cytometry. Cells were allowed to proliferate for 24 hours, and then were washed twice with dPBS and lysed using lysis buffer provided by the Thermo Scientific Active Ras Pull-Down and Detection Kit (16117) and Halt protease and phosphatase inhibitor cocktail (Thermo Scientific 79440). Samples were collected into 1.5mL microcentrifuge tubes and clarified by centrifugation at 16,000 x g at 4°C for 15 minutes. Supernatants were transferred to separate microcentrifuge tubes and protein concentration was determined by BCA assay (Thermo Scientific, 23225). 100µL 50% resin slurry was added to each spin cup, centrifuged at 6,000 x g for 30 seconds, and then

washed three times with 400µL kit lysis/wash buffer by gently inverting the tubes, centrifuging, and discarding the flow-through. 80µg aliquots of kit-provided GST-RAF1 RBD was added to the spin cups, followed by 300µg lysate in 500µL total volume of lysis/wash buffer. This was incubated for 1 hour at 4°C. Samples were then washed three times in lysis/wash buffer as described above, and eluted using 50µL kit-provided sample buffer with 200mM dithiothreitol (DTT) incubated at room temperature for 2 minutes. Samples were centrifuged for 2 minutes at 6,000 x g, heated at 95°C for 5 minutes, and then stored at -20°C for later use along with original lysate samples. Both elution and lysate were analyzed by western blot.

Western Blotting

Samples were washed twice with dPBS and then lysed using lysis/wash buffer from Thermo Scientific's Active Ras Pull-Down and Detection Kit (16117). After clarification by centrifugation at 16,000 *x g* at 4°C for 15 minutes, samples were transferred to another tube and measured for protein concentration using Thermo Scientific's BCA kit (23225). 25µg protein was then combined with Bolt LDS 4x buffer (Life Technologies B0007), Bolt Sample Reducing 10x buffer (Life Technologies B009), and deionized water for a final volume of 30µL per sample per well. Samples were then loaded alongside Chameleon® Duo Pre-stained Protein Ladder (LI-COR 928-60000) onto Bolt 10-well 4-12% Bis-Tris Plus gels (Life Technologies NW04120BOX) in Bolt MES SDS running buffer (Life Technologies B0002), and run at 200V for 30 minutes. Proteins were transferred to nitrocellulose transfer stacks (Life Technologies IB23001)

via an iBlot 2 machine, and blocked using Intercept® blocking buffer (LI-COR, 927-60001).

Primary antibodies were incubated overnight at 4°C, washed three times for 5 minutes in 0.05% Tween-20 TBS, and then incubated at room temperature in secondary antibody for 1 hour. Membranes were then washed again, read, and analyzed using LI-COR Odyssey and Imaging Software. The following primary and secondary antibodies were used:

Primary antibodies:	**Product No.**	**Dilution:**
MEK 1/2 mouse	Cell Signaling, 4694S	1:1000
Phospho-MEK 1/2 rabbit	Cell Signaling, 9154S	1:1000
Vinculin mouse	Sigma-aldrich V9131	1:1000
GFP mouse	Cell Signaling, 2955S	1:1000
Phospho-p70 S6 kinase rabbit	Cell Signaling, 9208T	1:1000
AKT mouse	Cell Signaling, 2920S	1:1000
Phospho-AKT Ser473 rabbit	Cell Signaling, 4060S	1:1000
pan-RAS mouse	Thermo Scientific, 16117	1:200
GFP rabbit	Cell Signaling, 2555S	1:1000
Phospho-ERK rabbit	Cell Signaling, 4370S	1:2000
ERK mouse	Cell Signaling, 9107S	1:1000
Secondary antibodies:	**Product No.**	**Dilution:**
Goat anti-Mouse IgG 680RD	LI-COR, 925-68070	1:10000
Goat anti-Rabbit IgG 800CW	LI-COR, 925-32211	1:10000

Table 2. Antibodies used in western blotting. List of antibody information and dilutions used.

Imaging

HEK293T cells were plated at 1.4e5 cells per well of a glass-bottom 6-well plate in 2mL phenol red-free DMEM (Life Technologies, 31053-028, 4.5g/L Glucose, 3.7g/L Sodium Bicarbonate), complete with 10% Tet screened FBS (Takara Bio, 631101) and 2mM L-Glutamine (Life Technologies, 25030081) and incubated at 37°C and 5% CO2. Cells were transfected the next day with 250ng of plasmids R705-M40-305 (mVenus-Hs.KRAS4b G12D), R714-M09-304 (mVenus-Hs.KRAS4b G12C), or R718-M86-305 (mVenus-Hs.KRAS4b) with a µg DNA to µL Fugene 6 ratio of 1 to 8. After 48 hours of incubation, confocal images were taken with a Nikon Eclipse Ti2. Images were processed in Fiji (Image J) using background subtraction and the sharpen processing tool(Schneider et al., 2012).

RESULTS

BRET assay optimization

The transfection parameters of time and Fugene 6:plasmid DNA ratio were first optimized for HEK293T cells. Cells were seeded at 1.4e5 cells per well of a 12-well plate in 1mL complete phenol red free DMEM, which yielded approximately 30% confluence on the day of transfection. Seeding at lower densities resulted in poor cell health after transfection. 50ng mVenus-KRAS4b G12D plasmid was cotransfected with 1ng RAF1(52-188)-NanoLuc with a 1:6 ratio of µg plasmid DNA to µL Fugene 6. Samples were incubated for either 24 or 48 hours and analyzed for NanoLuc and mVenus

expression separately as well as BRET signal (Figure 1A). Images were taken of cell confluency on the day of transfection and collection for each condition (Figure 1B).

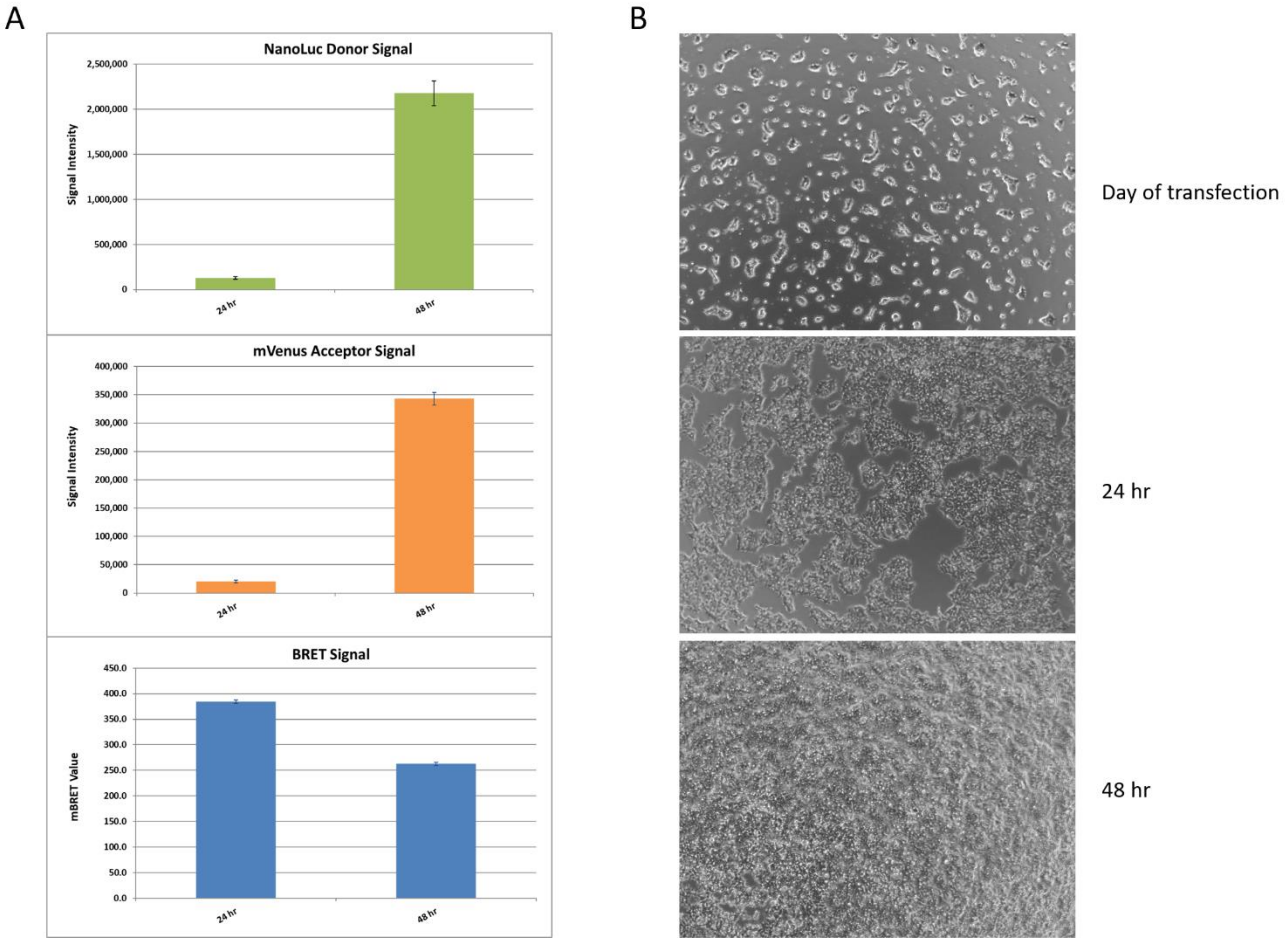

Figure 7. **Optimization of transfection duration.** (**a**) NanoLuc (460nm em), mVenus (500 ex; 530em), and BRET (530em/460em) signal was assessed in HEK293T cells cotransfected with mVenus-KRAS4b G12D (50ng) and RAF1(52-188)-NanoLuc (1ng) plasmid constructs. (**b**) Brightfield images of HEK293T cells on the day of transfection, 24 hours post-, and 48 hours post-transfection. Error bars show standard deviation from two separate biological replicates.

Cells were 70% confluent after 24 hours, and over 100% confluent after 48 hours. Both mVenus and NanoLuc signal was significantly higher at 48 hours, but BRET signal was suppressed. Transfection incubations of 24 hours were chosen for future experiments due to optimal confluency levels and BRET signal.

To assess ideal ratios of plasmid DNA to Fugene 6 for HEK293T cell transfection, the same amount of plasmid DNA was transfected using ratios ranging from 1:2 to 1:10. Signal was read after 24 hours (Figure 8). BRET signal—a ratiometric readout between resonance energy transfer emissions and donor-only emissions—remained relatively stable, but the expression of both mVenus-KRAS4b G12D and RAF1(52-188)-NanoLuc steadily increased with increasing DNA:Fugene 6 ratios. Transfection efficiency peaked with a 1:8 ratio, and reduced slightly when using a 1:10 ratio. DNA:Fugene 6 ratios of 1:8 were chosen for future experiments.

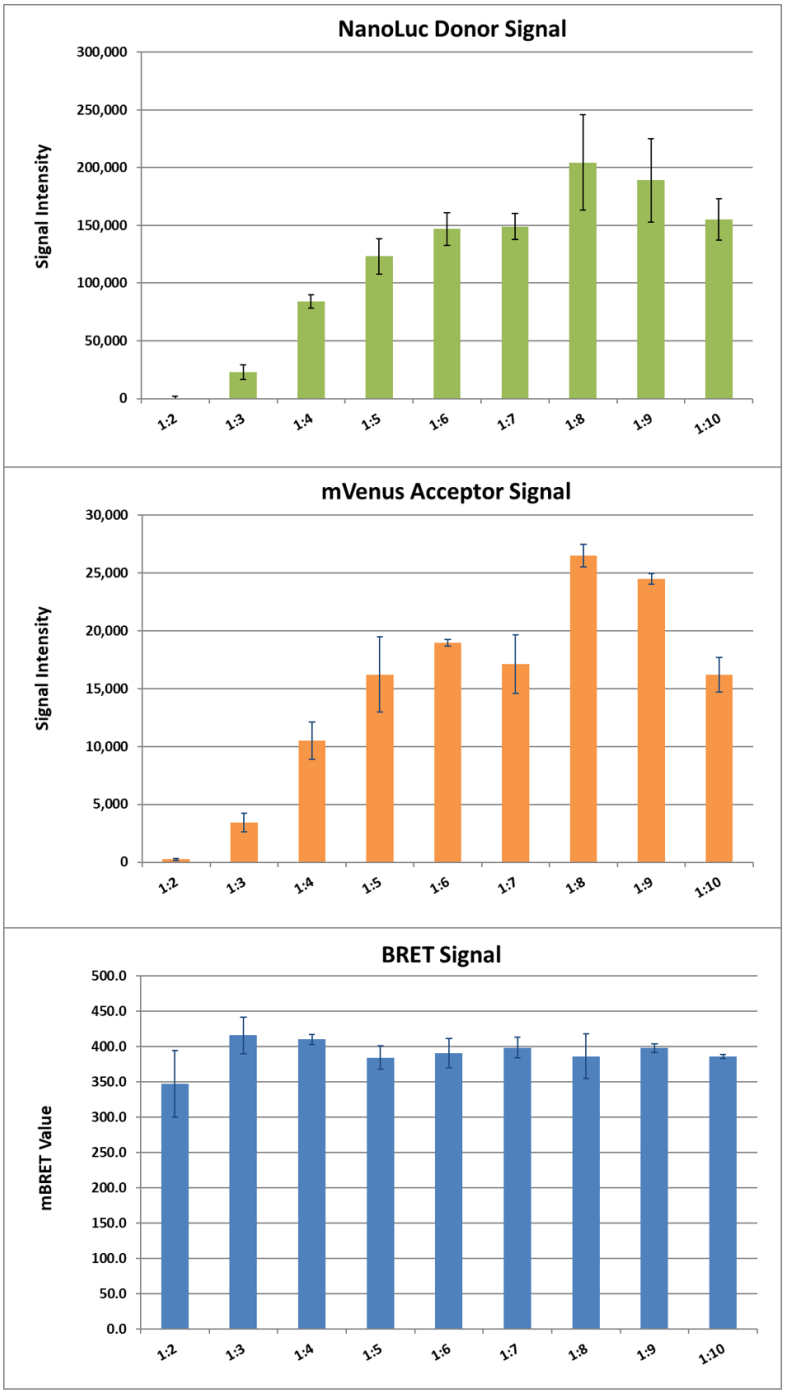

Figure 8. **Optimization of Fugene 6: Plasmid DNA ratios.** NanoLuc (460nm em), mVenus (500 ex; 530em), and BRET (530em/460em) signal was assessed in HEK293T cells cotransfected with mVenus-KRAS4b G12D (50ng) and RAF1(52-188)-NanoLuc (1ng) plasmid constructs with varying ratios of µg DNA: µL Fugene 6. Error bars show standard deviation from two technical replicates.

Because the efficiency of resonance energy transfer is a function of dipole-dipole orientation and distance, tag placement is critical for BRET readout (Pfleger and Eidne, 2006). All possible tag pairs should be tested to determine optimal BRET signal. RAS proteins require farnesylation of the c-terminal cysteine for membrane localization and efficient effector binding, and are therefore limited to n-terminal tags. Single-concentration co-transfections of all possible protein tag combinations in HEK293T cells were performed to determine the ideal BRET pair (Table 3, Figure 1). Both full-length RAF1 and the truncated RBD-CRD region of RAF1 (residues 52-188) were chosen to assess KRAS mutant binding affinity.

Donor	Acceptor
NL-RAF1(52-188)	mV-KRAS4b G12D
RAF1(52-188)-NL	mV-KRAS4b G12D
NL-RAF1	mV-KRAS4b G12D
RAF1-NL	mV-KRAS4b G12D
NL-p110a	mV-KRAS4b G12D
p110a-NL	mV-KRAS4b G12D
NL-KRAS4b G12D	mV-RAF1(52-188)
NL-KRAS4b G12D	RAF1(52-188)-mV
NL-KRAS4b G12D	mV-RAF1
NL-KRAS4b G12D	RAF1-mV
NL-KRAS4b G12D	mV-p110a
NL-KRAS4b G12D	p110a-mV

Table 3. **NanoLuc- and mVenus-tagged construct pairs to be evaluated.** NanoLuc donor (NL) and mVenus acceptor (mV) pairs to be co-transfected to determine optimal tag placement

5ng of each NanoLuc donor construct was cotransfected with 50ng of each mVenus construct into HEK293T cells and assessed for NanoLuc and mVenus

expression, separately, and BRET signal (Figure 9). Adequate expression of all NanoLuc constructs was seen except for p110α-NanoLuc, which was virtually undetectable.

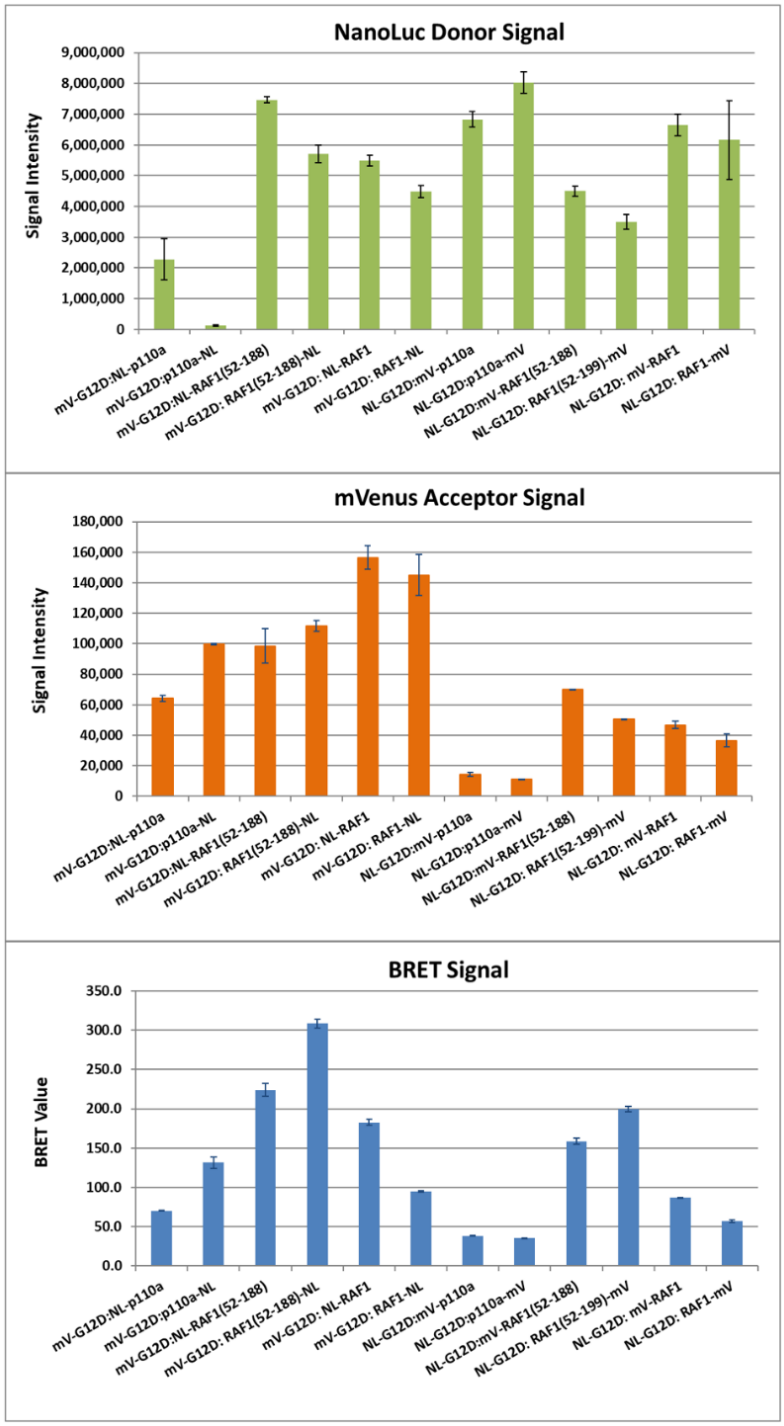

Figure 9. **Optimization of tag orientation.** NanoLuc (460nm em), mVenus (500 ex; 530em), and BRET (530em/460em) signal from single point transfections of all possible tag orientations between mVenus and NanoLuc constructs in Table 3. Error bars show standard deviations from two separate biological replicates.

Similarly, adequate expression of all mVenus constructs was seen except for mVenus-p110α and p110α-mVenus, which showed low expression. C-terminally tagged RAF1(52-188) produced higher BRET signal than the n-terminally tagged protein in both tag combinations, although the c-terminally tagged NanoLuc construct in combination with mVenus-KRAS4b G12D performed optimally. N-terminally tagged NanoLuc full-length RAF1 in combination with mVenus-KRAS4b G12D proved the ideal combination for this pair. While the BRET signal for c-terminally tagged NanoLuc p110α yielded the highest BRET signal, the n-terminally tagged construct was chosen due to exceedingly poor expression of the p110α-NanoLuc construct.

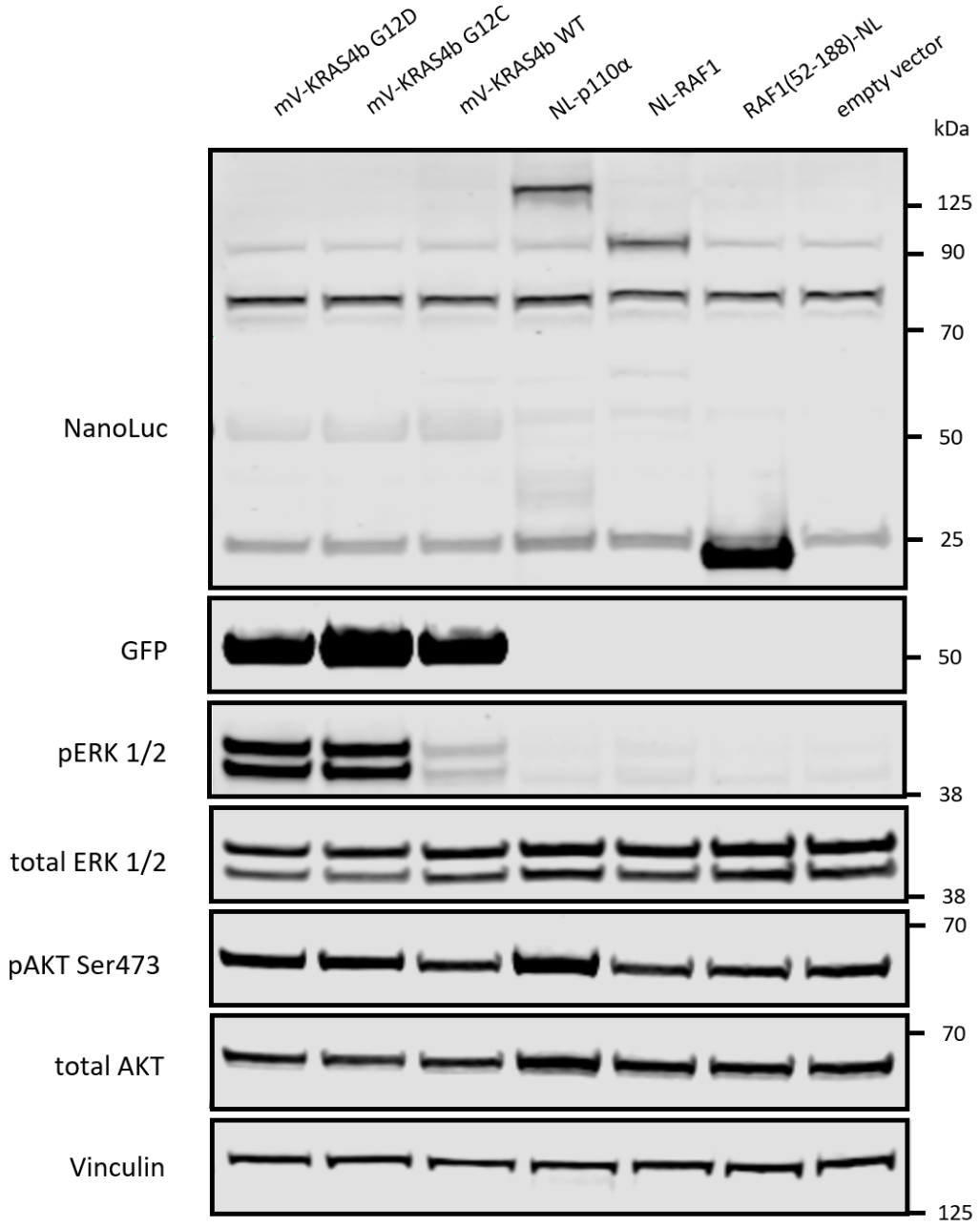

Figure 10. **Construct expression and activity.** Expression and downstream signaling of HEK293T cells transfected with 1µg of mVenus-KRAS4b or NanoLuc-tagged effector constructs.

When overexpressing exogenous constructs in a cellular system, it is necessary to validate that tag placement does not interfere with protein function or expression. Western blots of transiently expressed plasmids detected construct expression at the correct size for each chosen fusion protein (Figure 10). Overexpression of oncogenic constructs mVenus-KRAS4b G12D and mVenus-KRAS4b G12C caused marked overactivation of the MAP Kinase pathway as measured by ERK phosphorylation (Figure 10). Wildtype mVenus-KRAS4b activated ERK but to a lesser extent, while expression of NL-RAF1 caused marginal activation. Overexpression of NanoLuc-p110α led to higher levels of both total and phosphor-AKT in HEK293T cells. RAF1(52-188)-NanoLuc had no effect on downstream signaling, as expected for a functionally dead truncated fusion protein.

It is also necessary to determine the optimal level of donor construct to transfect for each saturation curve pair. Excess unbound donor increases background and reduces BRET signal. However, if donor expression is too low, BRET signal is subject to a higher degree of variation (noise). Saturation curves with varying donor expression levels were performed for each BRET pair (Figure 11), and 1ng RAF1(52-188)-NanoLuc and 5ng NanoLuc-p110α was determined to be ideal. Full-length RAF1 curves did not display saturation behavior, but rather had a hook effect at higher concentrations, and so were not evaluated in subsequent experiments (Figure 11).

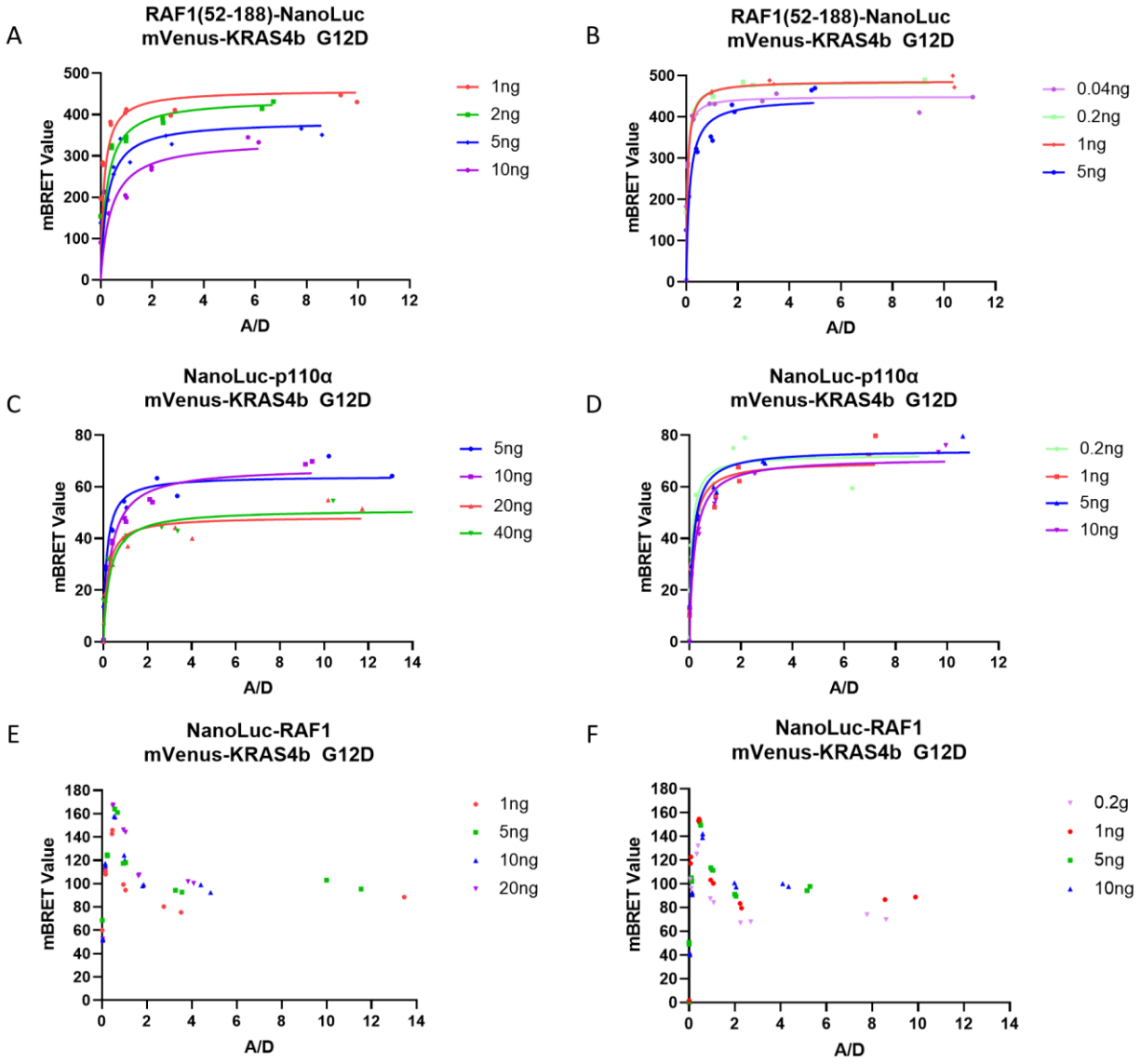

Figure 11. **Optimization of donor expression.** Saturation curves of mVenus-KRAS4b G12D acceptor constructs and NanoLuc-tagged effector donor constructs in HEK293T cells to determine optimum donor concentration. mVenus-KRAS4b G12D constructs were transfected in a 6-point half-log dilution curve with a top concentration of 1.2µg while NanoLuc-tagged constructs were held constant at the concentrations noted above.

HEK293T cells were transfected with mVenus-KRAS constructs and imaged to validate membrane localization (Figure 12). All constructs were seen to localize to the plasma membrane.

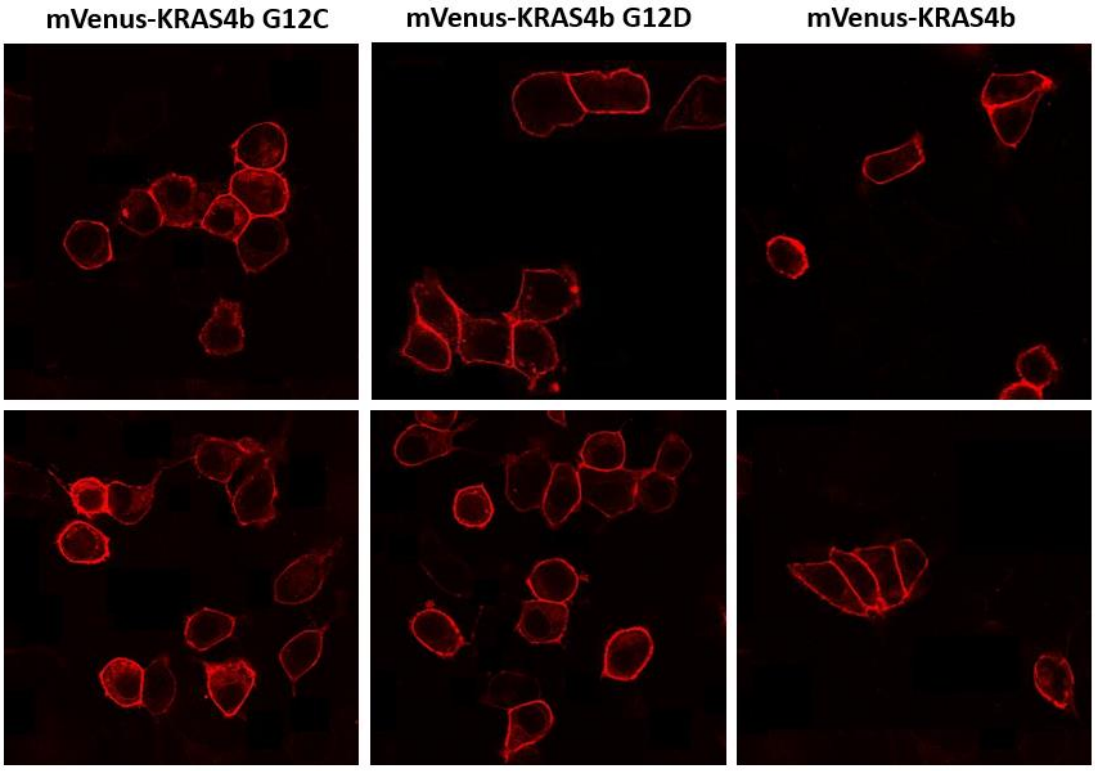

Figure 12. mVenus-RAS construct localization. HEK293T cells transiently transfected with mVenus-KRAS4b G12C, mVenus-KRAS4b G12D, or mVenus-KRAS4b constructs.

BRET saturation curves reveal differences in effector binding between oncogenic and wildtype KRAS but not between G12D and G12C mutants

Saturation curves between mVenus-KRAS4b G12D, mVenus-KRAS4b G12C, and mVenus-KRAS4b wildtype with the bioluminescently-tagged effector binding fragment RAF1(52-188)-NanoLuc revealed marked differnces in binding affinity between the mutant and wildtype proteins (Figure 13). Evaluation of binding with effector p110α revealed a similar pattern, with wildtype curves returning higher $BRET_{50}$ and lower $BRET_{max}$ values than mutant KRAS constructs (Figure 14). No discernable difference was observed between KRAS4b G12D and KRAS4b G12C mutants, however. RAS-binding deficient mutant controls RAF1(52-188)R89L and p110α T208D/K227A were used as negative controls in all comparisons. Both $BRET_{max}$ and $BRET_{50}$ values were drastically reduced in these controls; however, slight selectivity remained for the active mutants in both constructs as seen by the hyperbolic curve fit in contrast to the wildtype's linear increase typical of non-specific, random interactions.

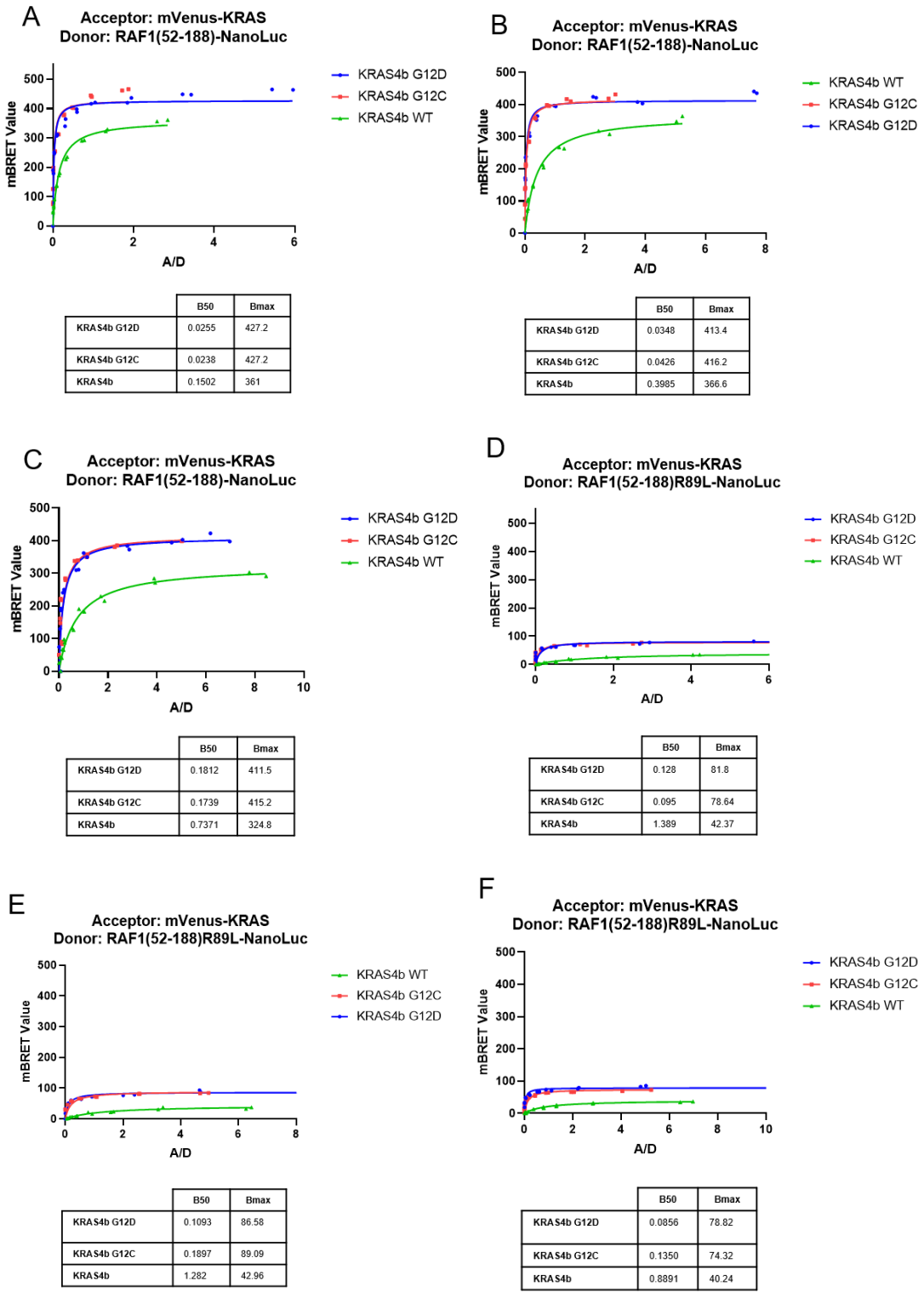

Figure 13. BRET saturation curves of RAF RBDCRD. Saturation curves between acceptor mVenus-KRAS4b constructs and donor NanoLuc constructs linked to the RAS binding domain and cysteine rich domain (RBDCRD) of the effector RAF1 (region 52-188) in HEK293T cells. mBRET values reflect the degree of bioluminesncene resonance energy transfer detected while

acceptor/donor values represent the relative expression levels of mVenus acceptor over constant levels of NanoLuc donor. Results from three separate biological replicates are shown in panels **a**, **b**, and **c**, along with extrapolated $BRET_{50}$ and $BRET_{max}$ values (determined by hyperbolic curve fit in GraphPad Prism). The R89L mutant, incapable of binding to RAS, is shown as a control in panels **d**, **e**, and **f**.

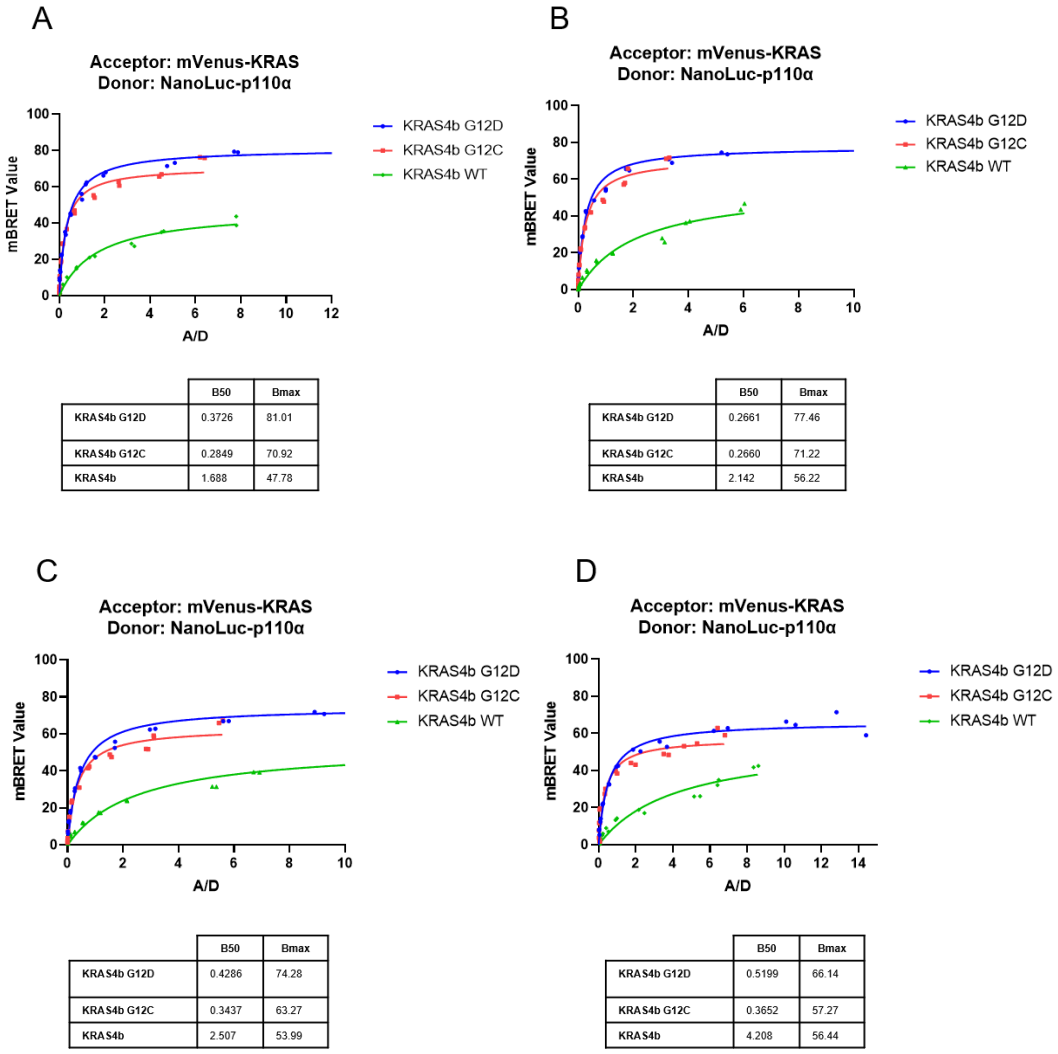

	B50	Bmax
KRAS4b G12D	0.3726	81.01
KRAS4b G12C	0.2849	70.92
KRAS4b	1.688	47.78

	B50	Bmax
KRAS4b G12D	0.2661	77.46
KRAS4b G12C	0.2660	71.22
KRAS4b	2.142	56.22

	B50	Bmax
KRAS4b G12D	0.4286	74.28
KRAS4b G12C	0.3437	63.27
KRAS4b	2.507	53.99

	B50	Bmax
KRAS4b G12D	0.5199	66.14
KRAS4b G12C	0.3652	57.27
KRAS4b	4.208	56.44

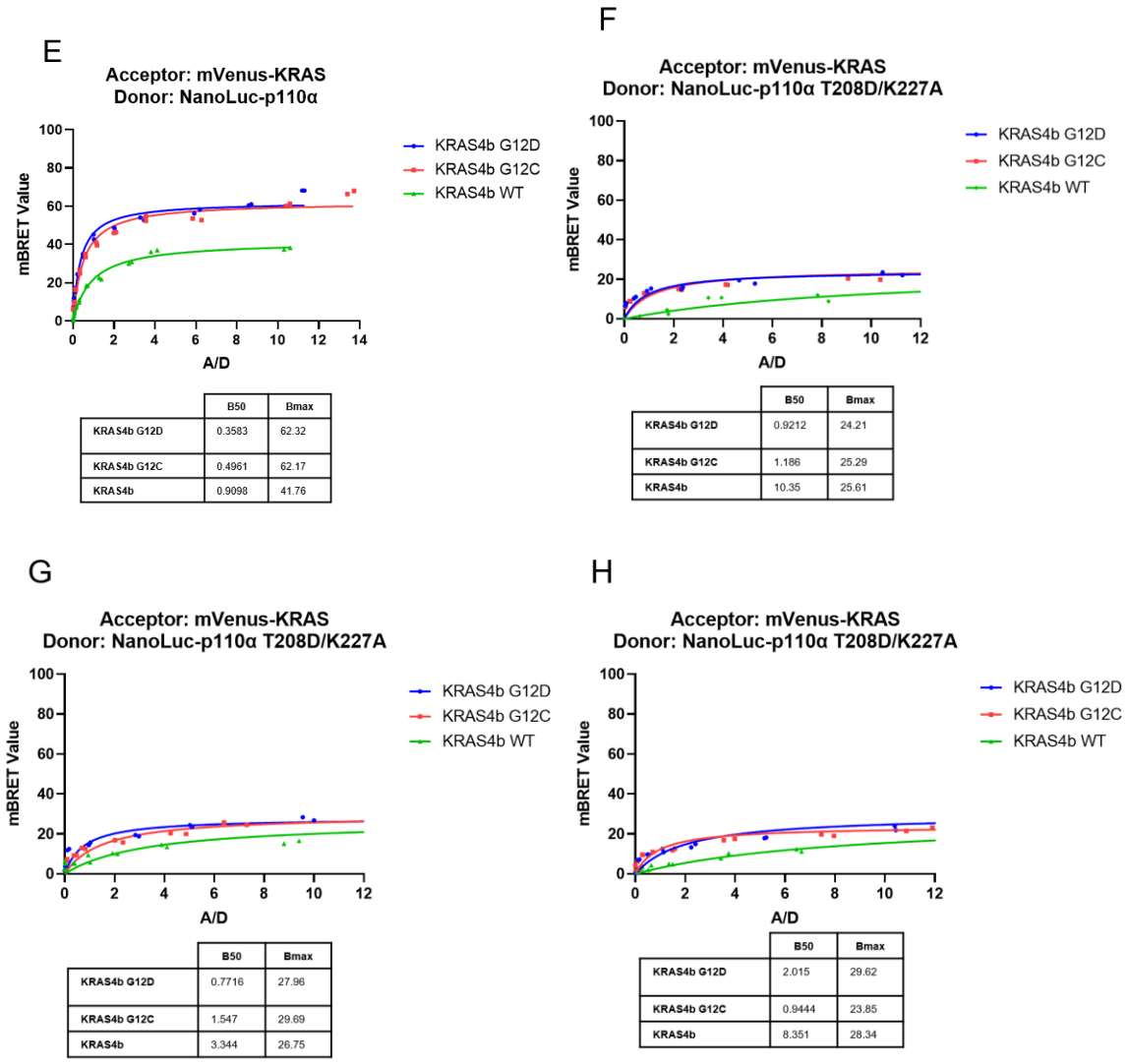

Figure 14. BRET saturation curves of p110α. BRET Saturation curves between acceptor mVenus-KRAS4b constructs and donor NanoLuc-tagged p110α constructs. Results from five separate biological replicates are shown in panels **a-e**, along with extrapolated $BRET_{50}$ and $BRET_{max}$ values (determined by hyperbolic curve fit in GraphPad Prism). The RAS binding deficient p110α T208D/K227A mutant is shown as a negative control in panels **f**, **g**, and **h**.

Evaluation of a panel of doxycycline-inducible RAS-mutant HeLa cell lines

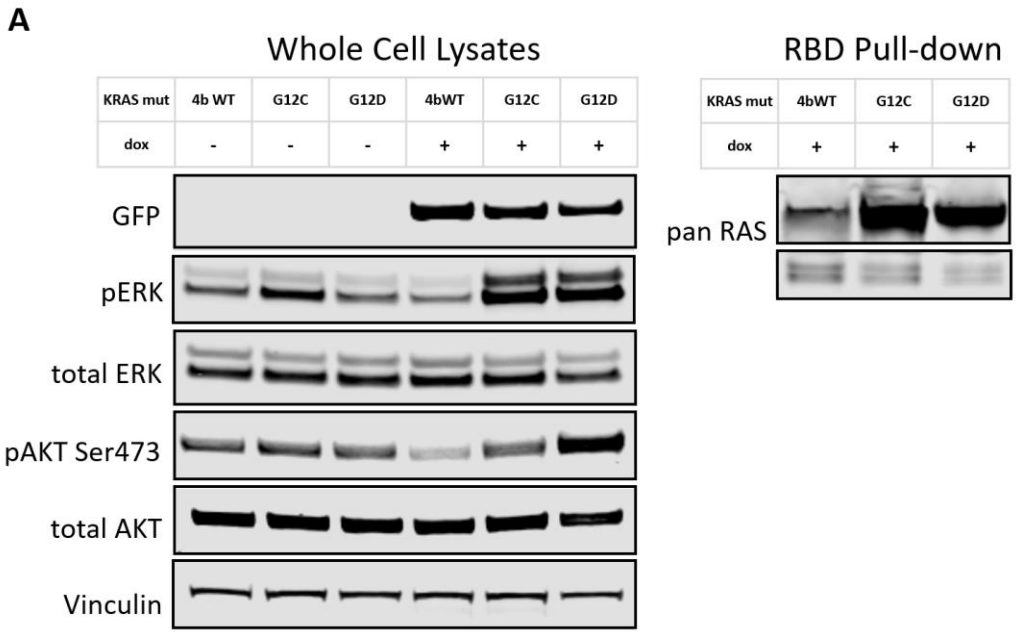

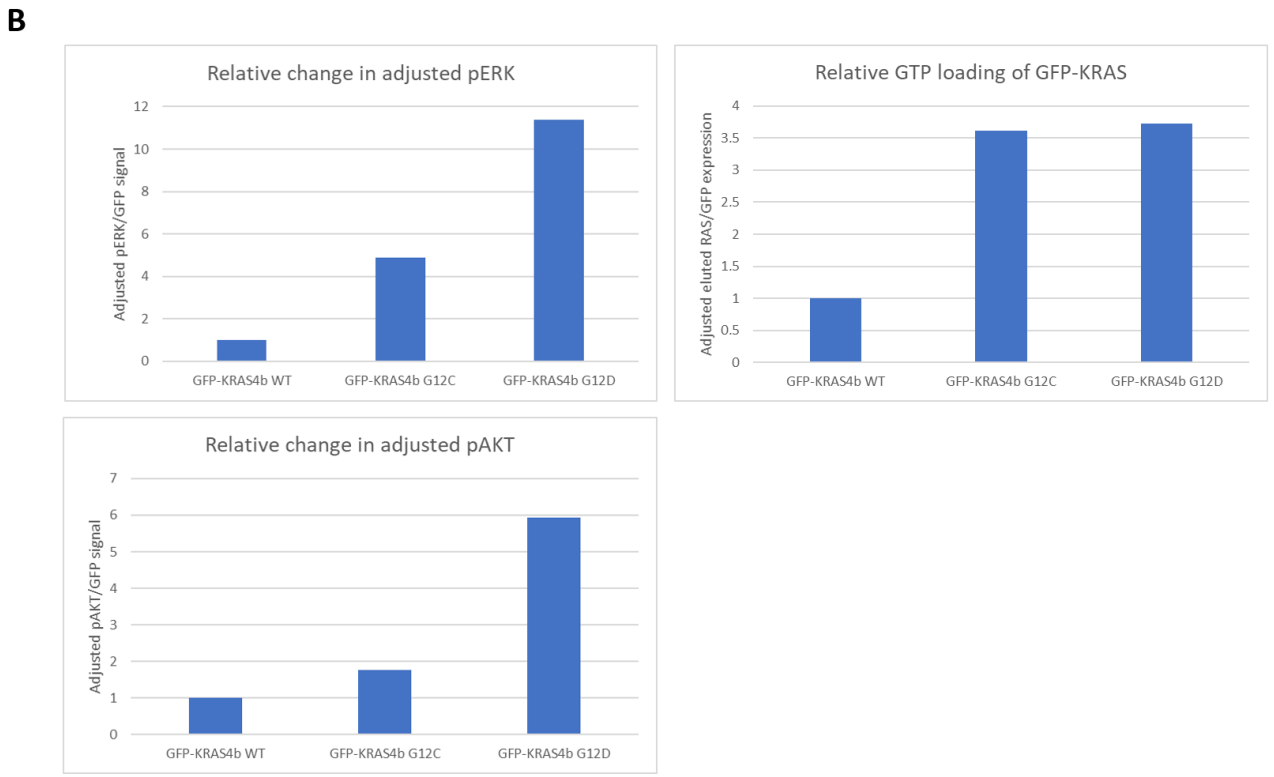

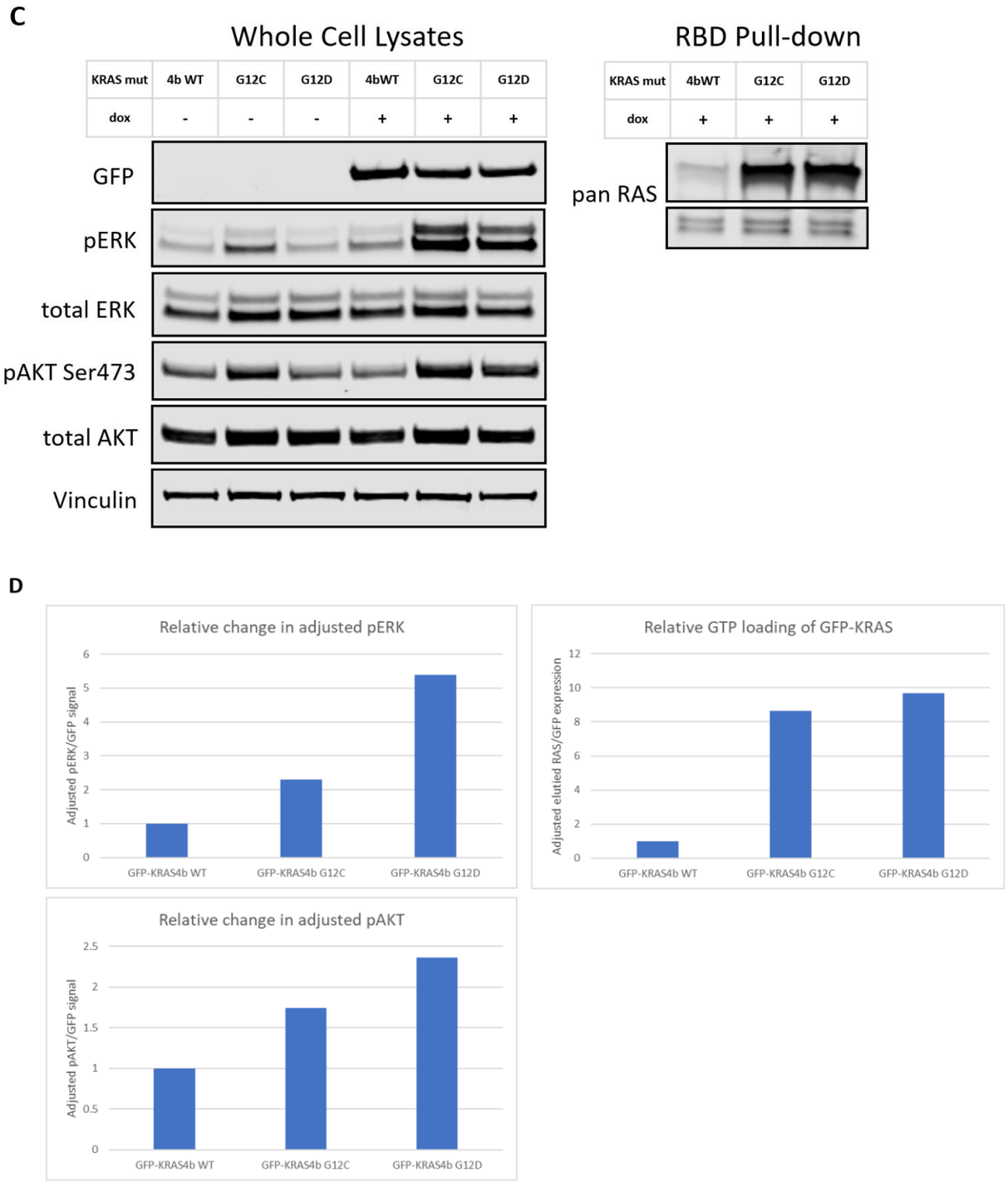

Figure 15. Active RAS pull-downs in a dox-inducible HeLa system. Evaluation of active RAS and downstream signaling levels in doxycycline-inducible HeLa cell lines (**a**). Densitometry for panel A is shown in panel (**b)**. Relative changes in ERK and AKT phosphorylation compared to non-dox controls was divided by GFP expression and

normalized to KRAS4b WT values. A second biological replicate is shown in panel (**c**), along with densitometry values in panel (**d**)

A doxycycline-inducible HeLa system was used to help determine differences in downstream signaling associated with KRAS4b G12D, KRAS4b G12C, and KRAS4b WT expression. Titration curves of doxycycline were first performed on HeLa cell lines using flow cytometry (data not shown) to normalize expression levels of GFP-tagged constructs for an accurate comparison. Cells were then subject to pull-downs utilizing an RBD fragment so as to only capture activated RAS. Relative levels of downstream activation were also evaluated via western blot in two biological replicates (Figure 15). Both KRAS4b G12D and KRAS4b G12C proteins showed increased activation compared to the wildtype, but no marked difference in GTP-loading was observed between mutants. Downstream phospho-MEK and phospho-ERK activation increased with expression of both mutant KRAS proteins (Figure 15). A higher induction of AKT phosphorylation at site serine 473 was observed with expression of KRAS4b G12D compared to KRAS4b G12C, and both mutant proteins activated AKT signaling to a greater extent than the wildtype.

GFP pull-downs revealed greater levels of p110α binding in the KRAS G12D line compared to the wildtype and G12C-mutant lines, and similar levels of RAF1 binding (Figure 16a). GFP-KRAS4b G12D HeLas exhibited greater AKT activation relative to KRAS4b G12C, KRAS4b WT, and HRAS WT driven lines, along with greater total activation of MEK and ERK, and higher phosphorylation of RAF1 at site S338 (Figure 16b).

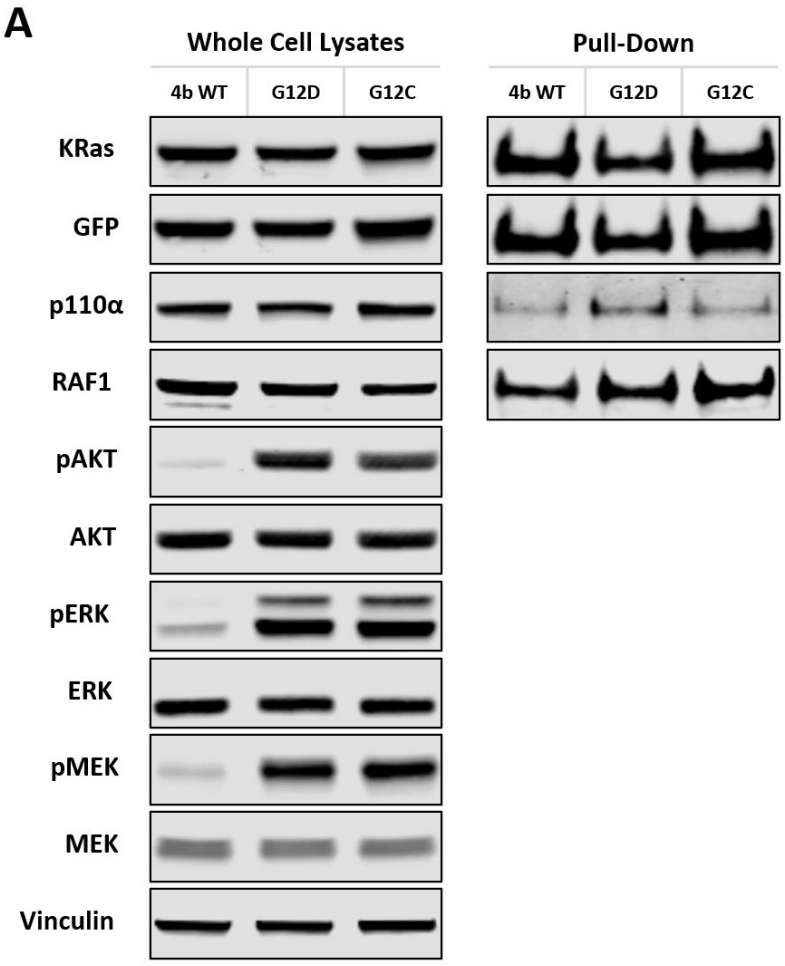
A
Whole Cell Lysates
Pull-Down
4b WT
G12D
G12C
4b WT
G12D
G12C
KRas
GFP
p110α
RAF1
pAKT
AKT
pERK
ERK
pMEK
MEK
Vinculin

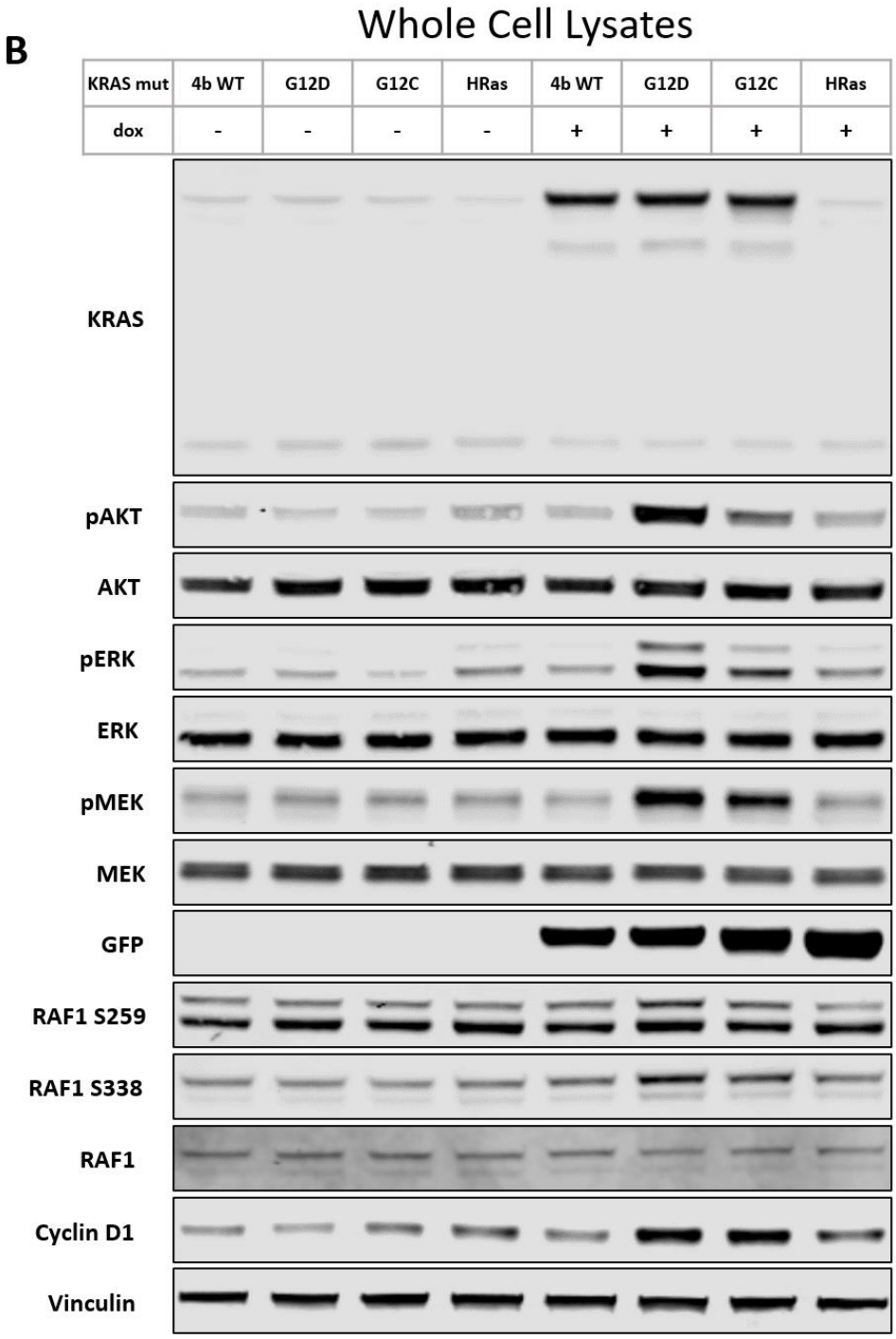

Figure 16. GFP pull-downs and signaling evaluation in a dox-inducible HeLa system. HeLa cell lines expressing a doxycycline-inducible GFP-tagged KRAS alleles were evaluated for basal signaling levels by western blot, and GFP-tagged constructs were pulled down using anti-GFP magnetic beads from Chromotek and evaluated for binding partners in two separate biological replicates (**a**). Basal signaling levels of several

GFP-KRAS mutant HeLa lines were compared and evaluated with and without doxycycline induction (**b**).

mVenus immunoprecipitation of KRAS mutant alleles shows higher p110α engagement in HEK293T cells

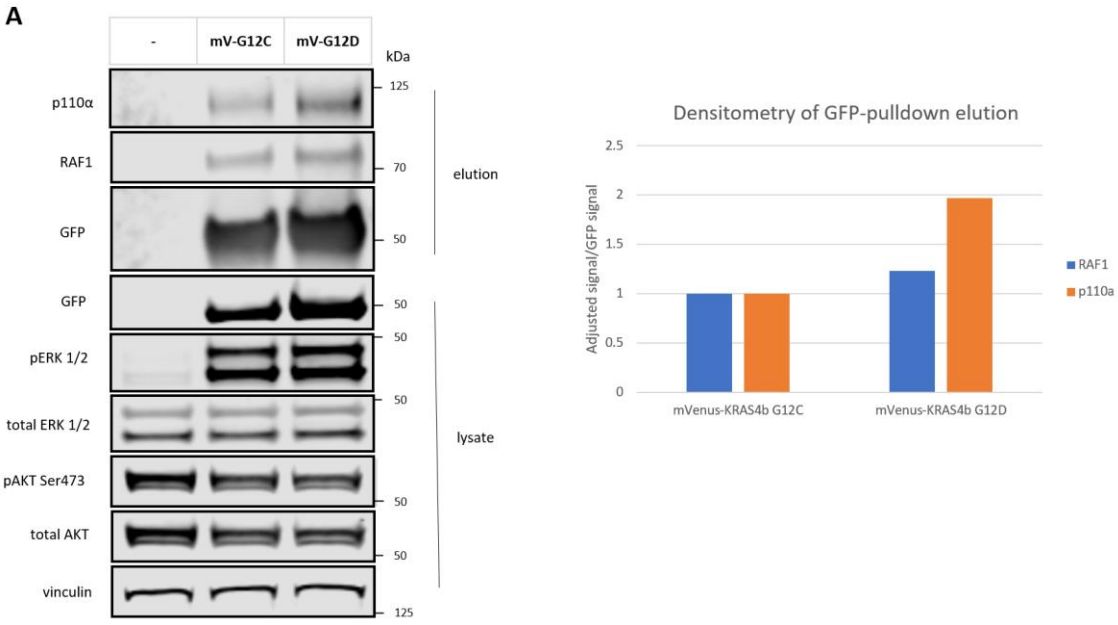

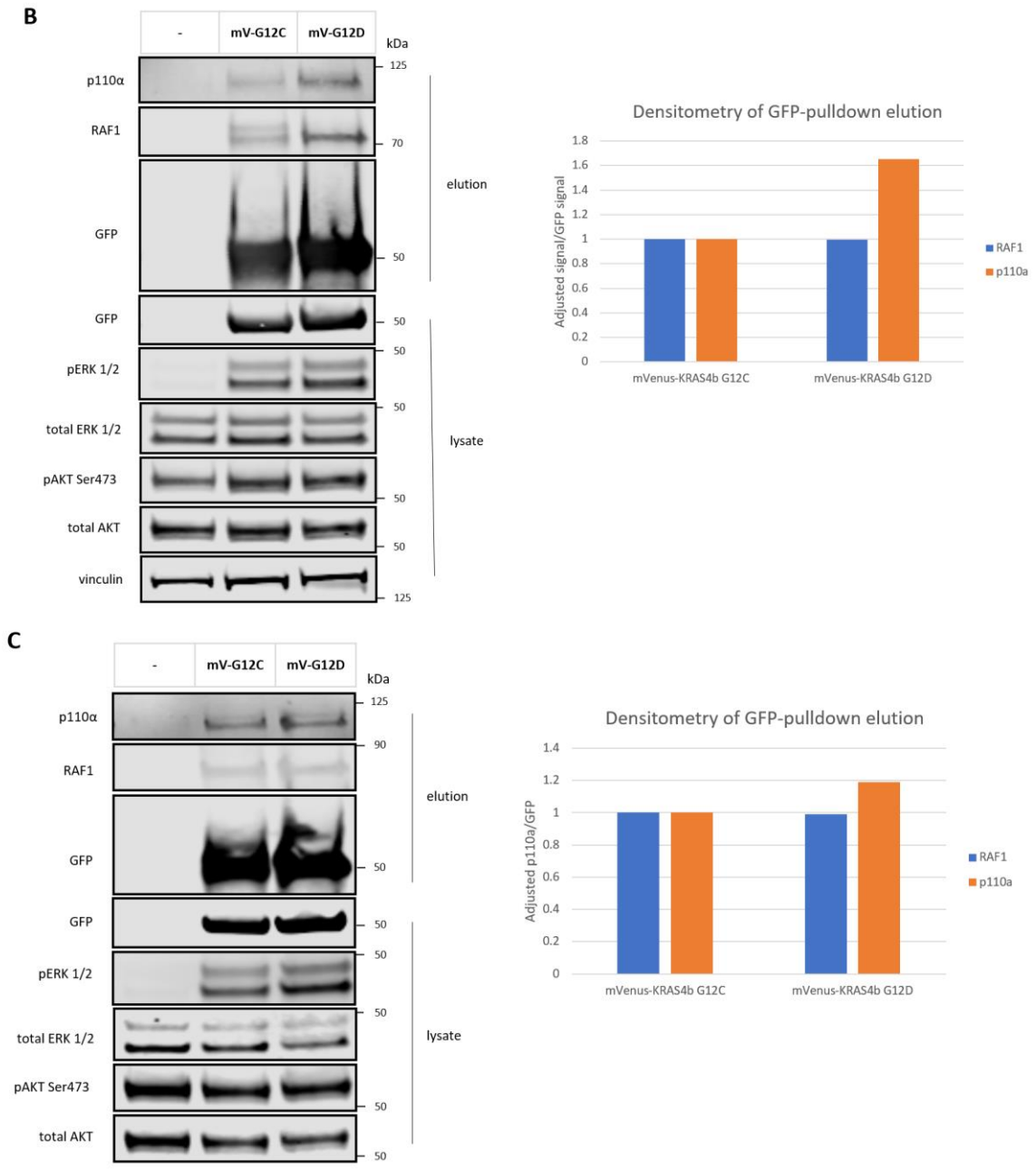

Figure 17. mVenus-RAS construct immunoprecipitation. GFP immunoprecipitation of mVenus-tagged (GFP derivative) KRAS4b G12C, G12D, or empty vector constructs transiently transfected into HEK293T cells in three separate biological replicates (panels **a, b,** and **c**). Normalized densitometry of eluted effector proteins are shown to the right of each western blot. Effector binding values were divided by GFP signal and normalized to KRAS4b G12C levels.

mVenus (a GFP derivative) tagged KRAS constructs were expressed in HEK293T cells and captured by immunoprecipitation utilizing GFP nanobodies coupled to magnetic agarose beads (Figure 17). Similar induction of phospho-ERK signaling was seen between G12D and G12C mutants (Figure 17). Similar levels of endogenous RAF1 were captured between mutants across biological replicates; however, slightly higher levels of endogenous p110α were observed in KRAS4b G12D samples as determined by densitometry measurements of the eluted proteins normalized to GFP. No difference in AKT activation was observed with mutant KRAS overexpression in HEK293T cells, likely because AKT is constitutively active in this cell line due to transformation with the SV40 large T antigen (Ramakrishnan et al., 2014).

RAF1(52-188)-KRAS4b G12D BRET saturation curves are affected by G12D inhibitor

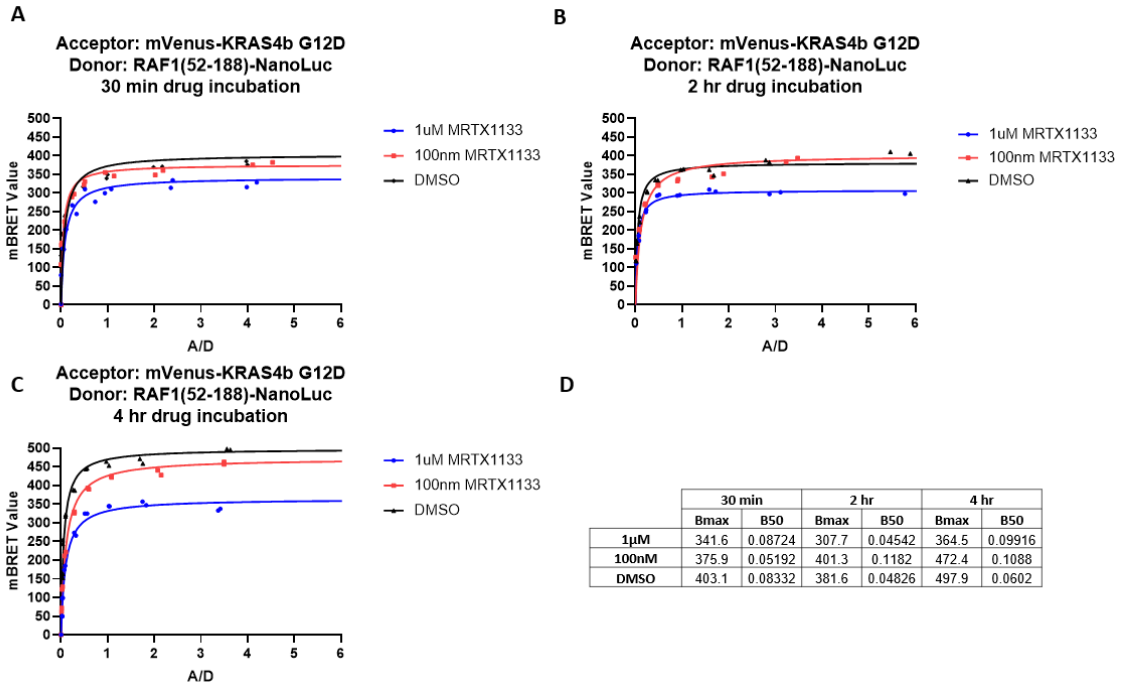

	30 min		2 hr		4 hr	
	Bmax	B50	Bmax	B50	Bmax	B50
1µM	341.6	0.08724	307.7	0.04542	364.5	0.09916
100nM	375.9	0.05192	401.3	0.1182	472.4	0.1088
DMSO	403.1	0.08332	381.6	0.04826	497.9	0.0602

Figure 18. KRAS4b G12D-RAF1 RBDCRD saturation curves with MRTX1133. mVenus-KRAS4b G12D and RAF1(52-188)-NanoLuc BRET Saturation curves were performed with 1µM and 100nM of non-covalent KRAS G12D inhibitor MRTX1133, along with a DMSO control, for incubation periods of 30 minutes (**a**), 2 hours (**b**), and 4 hours (**c**). $BRET_{max}$ and $BRET_{50}$ values are reported in panel (**d**).

BRET saturation curves between mVenus-KRAS4b G12D and RAF1(52-188)-NanoLuc were repeated following incubation with the non-covalent KRAS G12D-specific inhibitor MRTX1133 developed by Mirati Therapeutics (Christensen, 2021). Concentrations of 1µM, 100nM, or a DMSO control were incubated for 30 minute, 2 hour, and 4 hour timepoints (Figure 18). A depreciation of $BRET_{max}$ values was observed in the 1µM condition in all timepoints, and a right shift in $BRET_{50}$ values was seen in

both 100nM and 1μM after 4 hours of incubation, indicating a reduced affinity for the RAF1(52-188) effector upon drug treatment.

DISCUSSION

Biochemical measurements of protein affinity overlook crucial elements inherent to a physiological setting such as membrane interaction, subcellular localization, cofactor concentration, signaling feedback and crosstalk, and interaction with other proteins. Here, we propose a method of measuring relative protein affinity in HEK293T cells using BRET saturation curves between the bright bioluminescent donor tag NanoLuc and the monomeric fluorescent acceptor tag mVenus. Previous biochemical, cellular, and tissue-based studies have reported conflicting results regarding differences in effector affinity across oncogenic RAS mutations. Our optimized protocol captures interactions between KRAS4b and its effectors p110α and the RAS binding domain of RAF1 (residues 52-188) to investigate differences in effector binding preferences between the wildtype and mutant G12D and G12C proteins. Cell seeding density, transfection conditions, tag placement, and donor to acceptor ratios were optimized to compare relative affinities between these proteins with precision (Figures 7, 8, 9, and 11). Protein constructs were proven to express well in HEK293T cells, and KRAS4b constructs localized correctly to the plasma membrane (Figures 10 and 12).

Interestingly, during optimization we observed full-length RAF1 constructs to display a hook effect when evaluated by BRET saturation curves (Figure 11). Compared to RBDCRD alone, the full-length RAF1 protein contains autoinhibitory and kinase

domains capable of homo- and hetero-dimerization with other RAF isoforms. It is possible that at higher levels of RAS expression, negative feedback signaling dampens RAS-RAF interaction. Alternatively, heterodimerization may occur to a greater extent with increased RAS signaling, leading to fewer interactions between RAF1 and RAS.

When comparing relative affinities between mutants KRAS4b G12D and G12C to KRAS4b wildtype, we observed a significant difference in $BRET_{50}$ values for both p110α and RAF1 RBDCRD (see Table 4). However, no such difference in affinity for either effector was seen between mutants in HEK293T cells. Incubation with KRAS G12D-specific inhibitor MRTX1133 did yield higher $BRET_{50}$ and lower $BRET_{max}$ values after 4 hours, demonstrating the efficacy of our system in detecting relative interaction strength and affinity shifts (Figure 18).

	RAF1(52-188)	**RAF1(52-188)R89L**	**p110α**	**p110α T208D/K227A**
KRAS4b G12D vs KRAS4b G12C	0.7886	0.3034	0.5024	0.9828
KRAS4b G12D vs WT	0.0316	0.01656	0.0212	0.09446
KRAS4b G12C vs WT	0.0355	0.01764	0.0202	0.09791

Table 4. Statistical differences in $BRET_{50}$ values across BRET saturation curve biological replicates. Significance of comparison between $BRET_{50}$ values from BRET Saturation curves across biological replicates. Values were compared using a two-tailed paired t-test assuming unequal variance.

RAF1 RBDCRD (residues 52-188) exhibited similar binding behavior to both mutants KRAS4b G12D and KRAS4b G12C. This is in contrast to biochemical data generated by Hunter et al., who reported a significant decrease in affinity for RAF1-RBD(51-131) by KRAS4b G12D and a slight decrease by KRAS4b G12C as measured by a proximity-based luminescence competition assay (Hunter et al., 2015). As described

in Hunter et al., this decrease in affinity may be due to a reordering of the KRAS switch I region by G12 substitutions when in the closed, state 2 conformation (capable of binding effectors).

Results from our BRET analysis suggest that these differences seen in biochemical experiments may not translate to a cellular system, as we did not see any significant distinction between KRAS4b mutant binding behavior to RAF1(52-188). It is important to note that our comparison was made with the RBDCRD region of RAF1 rather than the RBD alone. The cysteine-rich domain (CRD) of RAF1 is reported to interact both with membrane phosphatidylserine lipid head groups and directly with KRAS (Bondeva et al., 2002; Terrell and Morrison, 2019; Tran et al., 2021). Importantly, our cellular system reflects the GTP/GDP ratio present in cells, in contrast to the non-hydrolyzable GTP analog GppNHp used in biochemical experiments. Thus, results from our BRET curves factor in intrinsic hydrolysis rates, along with cofactor concentration, membrane interactions, cellular feedback signaling, and interaction with regulatory proteins such as GEFs and GAPs. It is possible that within this complex environment, any slight differences seen between mutants in biochemical RAF1 binding data become undetectable. Additionally, the net sum of these cellular processes may yield equivalent activation and RAF1 binding activity between mutants, regardless of slight differences in biochemical properties. Indeed, Gillies et al. reported similar ERK output across several oncogenic KRAS mutations in isogenic mouse embryonic fibroblasts, finding variations in feedforward modulation of phosphatase activity and feedback strength that serve to rescale pathway sensitivity (Gillies et al., 2020). Our evaluation by RBD pull-down of GFP-tagged KRAS from a panel of doxycycline-inducible HeLa cells showed no

difference in KRAS activation between G12D and G12C mutants (Figure 15). Similar evaluation in transfected HEK293T cells was not performed.

Unexpectedly, the R89L mutant negative control, which purportedly prevents the RAS binding domain (RBD) from engaging with RAS (Dent et al., 1995), still displayed some degree of interaction with active RAS as observed in our system (Figure 13). While wildtype KRAS engaged with the R89L mutant in a linear fashion typical of non-specific binding, mutant KRAS constructs did interact with the protein in a hyperbolic curve indicative of specific binding, although $BRET_{max}$ values, and therefore total interactions, were markedly lower. This is reflected in the significant difference in $BRET_{50}$ values between mutant KRAS4b and the wildtype protein when binding to RAF1(52-188) (Table 4). The specificity for constitutively active RAS over the wildtype does imply selective interaction and membrane recruitment of this mutant RAF1 fragment, despite the reported binding deficiency.

Similar to published biochemical data, we observed the relative affinity of KRAS4b proteins for p110α to be lower than that of RAF1 RBDCRD (Pacold et al., 2000; Burge and Hobbs, 2022). However, we did not see a significant difference in affinity between the oncogenic mutants (Table 4). Like the RAF1(52-188) R89L mutant that supposedly does not interact with RAS, the PIK3CA T208D/K227A reportedly prevents RAS binding but also showed a marginal affinity for the active KRAS mutants G12D and G12C over the wildtype, although the $BRET_{max}$ (total interactions) was much lower than with the wildtype effector (Figure 14) (Zhao and Vogt, 2010). When comparing $BRET_{50}$ values of this mutant negative control, both active KRAS G12D and KRAS G12C were significantly different to the wildtype, suggesting that the interaction

is also due to specific recruitment by active RAS and not to random, bystander BRET interactions (Table 4). However, because our BRET technique cannot distinguish between subcellular compartments, it is impossible to discern whether this interaction is occurring at the plasma membrane, or within the crowded endomembrane environment during translation and as an artefact of overexpression.

While no statistical difference was seen in direct p110α engagement between mutants, we did observe evidence of greater p110α engagement and downstream signaling by the KRAS4b G12D mutant through other methods. GFP pull-downs of GFP-KRAS4b G12D captured more endogenous p110α than GFP-KRAS4b G12C or GFP-KRAS4b wildtype in doxycycline-inducible HeLa cell lines, whereas captured RAF1 showed no difference (Figure 16). Pull-downs of mVenus-KRAS4b G12D constructs in HEK293T cells also captured higher levels of p110α relative to mVenus-KRAS4b G12C (Figure 17). Eluted RAF1 showed no difference between mutants (Figure 17). It is possible that there exists a marginal difference in p110α affinity that cannot be detected within the range of the BRET system. Membrane recruitment and transition from a 3D to 2D environment is the equivalent of a five orders of magnitude increase in binding constant for GEFs and GAPs (Simanshu et al., 2017). With such a great increase in concentration and binding activity brought by membrane recruitment, our BRET saturation curve method may render subtle differences in binding affinity for p110α difficult to distinguish. Additionally, any slight differences present may be within the margins of error of our assay.

Signaling data from dox-inducible HeLa cells suggests a higher relative increase in AKT phosphorylation with KRAS4b G12D expression compared to G12C (Figure 15,

16). In contrast, AKT signaling in HEK293Ts remains constitutively active due to expression of the SV40 large T antigen, and no such difference was observed in this cell line (Figure 17) (Ramakrishnan et al., 2014). We also observed greater AKT activation in a panel of oncogenic cell lines driven by *KRAS G12D* mutations when compared to *G12C, G12V,* and *G12R* mutations (Figure 19). This is supported by existing data where both *KRAS G12D*-mutant cell lines and tumor models show a greater propensity for AKT signaling than those carrying a mutant *G12C* allele (Floyd et al., 2005; Ihle et al., 2012). NSCLC cell lines with *G12D* mutations show enhanced AKT signaling, while *G12C* lines have decreased growth factor-induced activation of AKT (Ihle et al., 2012; Riquelme et al., 2016). *In vivo* data show KRAS4b G12C-driven mouse lung cancer models to have increased MAPK but not AKT signaling (Floyd et al., 2005). From patient tumor data, 90% of pancreatic cancers harbor *KRAS* mutations, the majority of which are *G12D* (Prior et al., 2020). Increased PI3K activity is associated with up to 60% of all PDAC cases, which is also linked to poorer prognosis (Ebrahimi et al., 2017). Despite this body of evidence, biochemical data showing a clear comparison in p110α binding between G12D and other KRAS mutants has yet to be published.

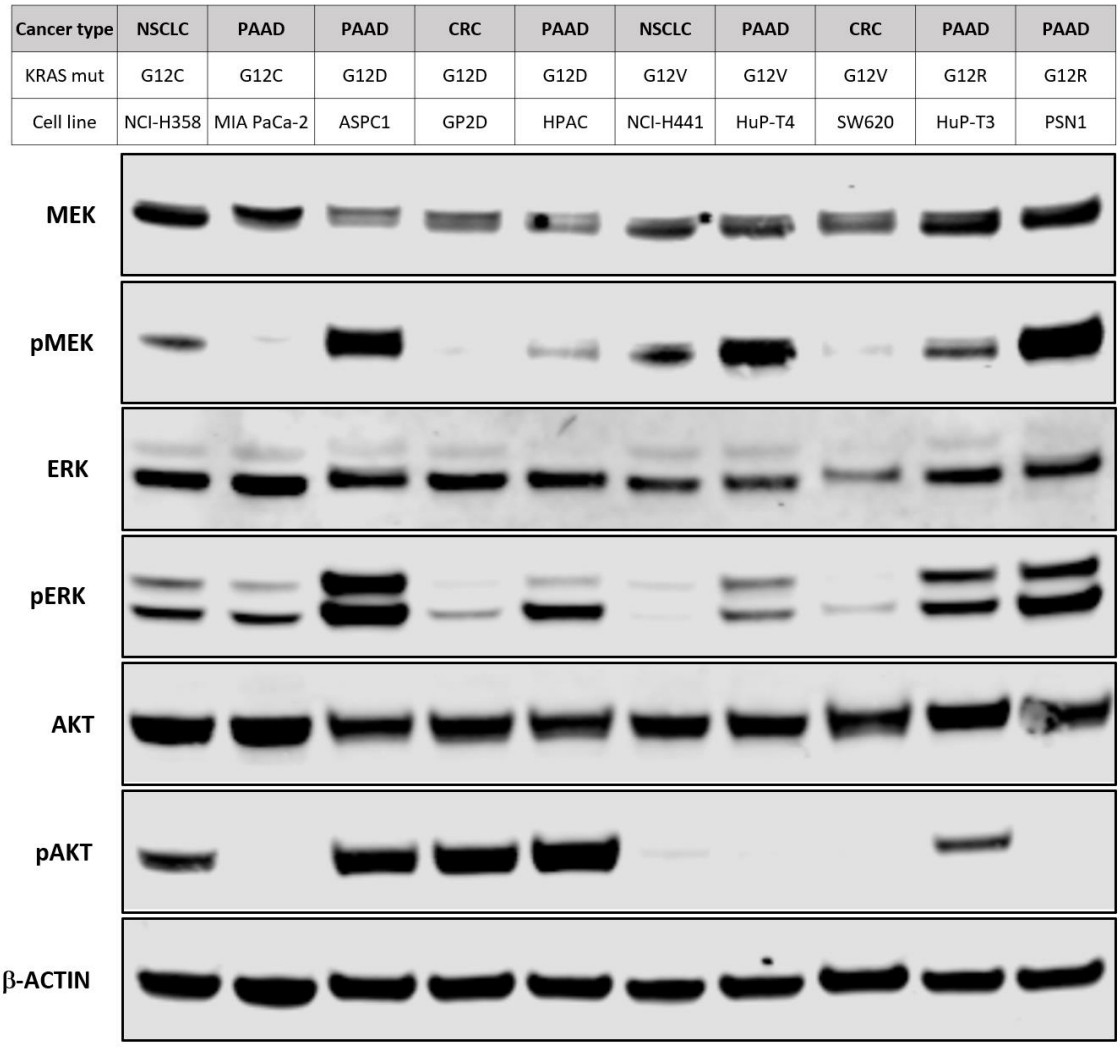

Figure 19. KRAS-driven oncogenic cell line signaling. Basal signaling levels in a panel of oncogenic cell lines as measured by western blot.

While we did not observe statistical differences in cellular binding behavior, investigation into solution-state NMR structures did reveal differences between KRAS4b G12D, KRAS4b G12C, and KRAS4b wildtype proteins in the active (GppNHp-bound) conformation.

Heteronuclear single quantum correlation (HSQC) spectroscopy is a highly sensitive and informative technique for studying protein structure. The amide proton in

each amino acid's backbone (minus proline) is magnetized and transfers its energy to the neighboring nitrogen, which then returns after a time delay and is measured. ^{1}H and ^{15}N chemical shifts within each amino acid are dependent on its unique chemical environment within the folded protein, and two-dimensional plots of these spectra represent the protein's 'fingerprint.' In contrast to the artificial conditions inherent to X-ray crystallography such as pH and salt concentration, structural data from solution-state NMR more reliably captures the subtle, dynamic properties of proteins in their natural state. We compared G12D, G12C, and wildtype KRAS constructs (AA 1-169) using ^{1}H–^{15}N HSQC spectroscopy.

Superimposition of the two-dimensional ^{1}H–^{15}N HSQC spectra of both KRAS4b G12C and KRAS4b G12D over the wildtype revealed significant chemical shift perturbations (CSP) for select residues (Figure 20). Ten residues in the G12D protein exhibited CSPs compared to the wildtype: P-loop amino acids D12, G13, and K16, and residues G60-64, A66, and Y71 in the switch II region (Figure 20). Eight amino acids showed similar perturbations when comparing G12C and wildtype spectra: C12, G13, K16, and G60-Y64. In this comparison, A66 and Y71 adopted the same positions as in the wildtype protein. Except for Q61 and G12C, CSP residues found in both KRAS4b G12D and G12C spectra were significantly more perturbed in the former. The G12D vs. WT comparison yielded a higher threshold CSP value ($\Delta\delta_{cutoff}$ 0.096) than G12C vs. WT (0.053), suggesting larger degree conformational differences across this mutant protein. CSPs between G12-mutant and wildtype proteins within P-loop residues may be due to local effects of the G12 mutation; however, clear differences in CSPs across switch II residues suggest that the G12C and G12D mutations induce distinct conformations.

Similar findings were reported in a solution-state NMR study comparing GDP-bound KRAS4b G12C, G12D, G12V, and wildtype, with KRAS G12D-GDP inducing unique and significant perturbations in P-loop and switch II residues (Pálfy et al., 2020).

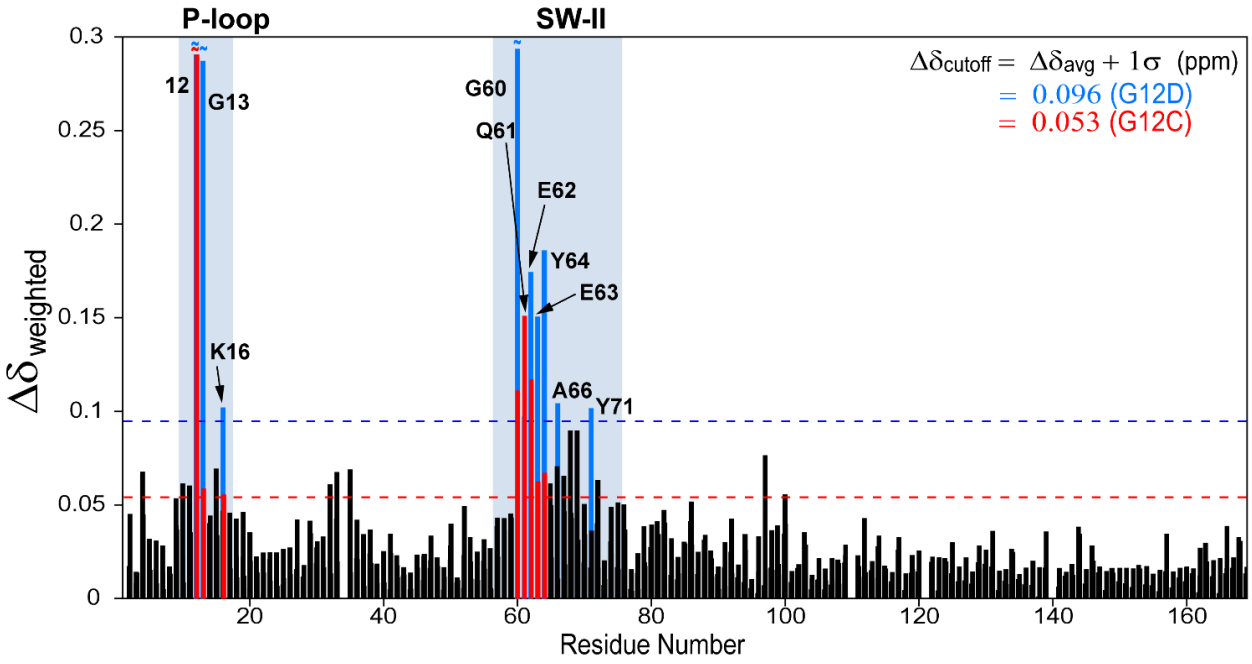

Figure 20. Chemical shift perturbations between mutant and wildtype KRAS. The plot of $^{1}H^{N}$ and ^{15}N chemical shift difference ($\Delta\delta_{weighted}$) vs residue number between KRAS wildtype-GppNHp (BMRB ID 50651) and KRAS G12C -GppNHp, and between KRAS wildtype-GppNHp and KRAS G12D -GppNHp. Significant difference in Δδ of highlighted residues (rendered red for WT vs G12C and blue for WT vs G12D; above the respective threshold value) between the two proteins likely reflect mutation-induced conformational changes. Threshold value ($\Delta\delta_{cutoff}$) is represented as horizontal dashed line (shown in red for G12C and in blue for G12D)

Molecular Dynamics (MD) simulations of RAS structures confirmed differences between KRAS mutants. GppNHp-bound KRAS4b, KRAS4b G12C, and KRAS4b G12D structures were simulated and observed over a 2μs timeframe (Figure 21). RMSD of

protein backbones and GppNHp (Figure 21 panels a, b) indicate a stable dynamic run. Atomic fluctuations (root-mean-squared fluctuation, RMSF) within residues of each protein were then calculated. Switch I (aa 32-38) and switch II (aa 59-67) regions exhibited dynamic behavior across all proteins (Figure 21 c). KRAS4b G12D displayed more dynamic behavior in loop region 101-109 relative to other protein models (Figure 21 c). These observations align with our structural NMR data and suggest that the G12D mutation confers greater flexibility in the switch II region, and may trigger some allosteric instability and alter the dynamics of loop 101-109 (Figure 21 c).

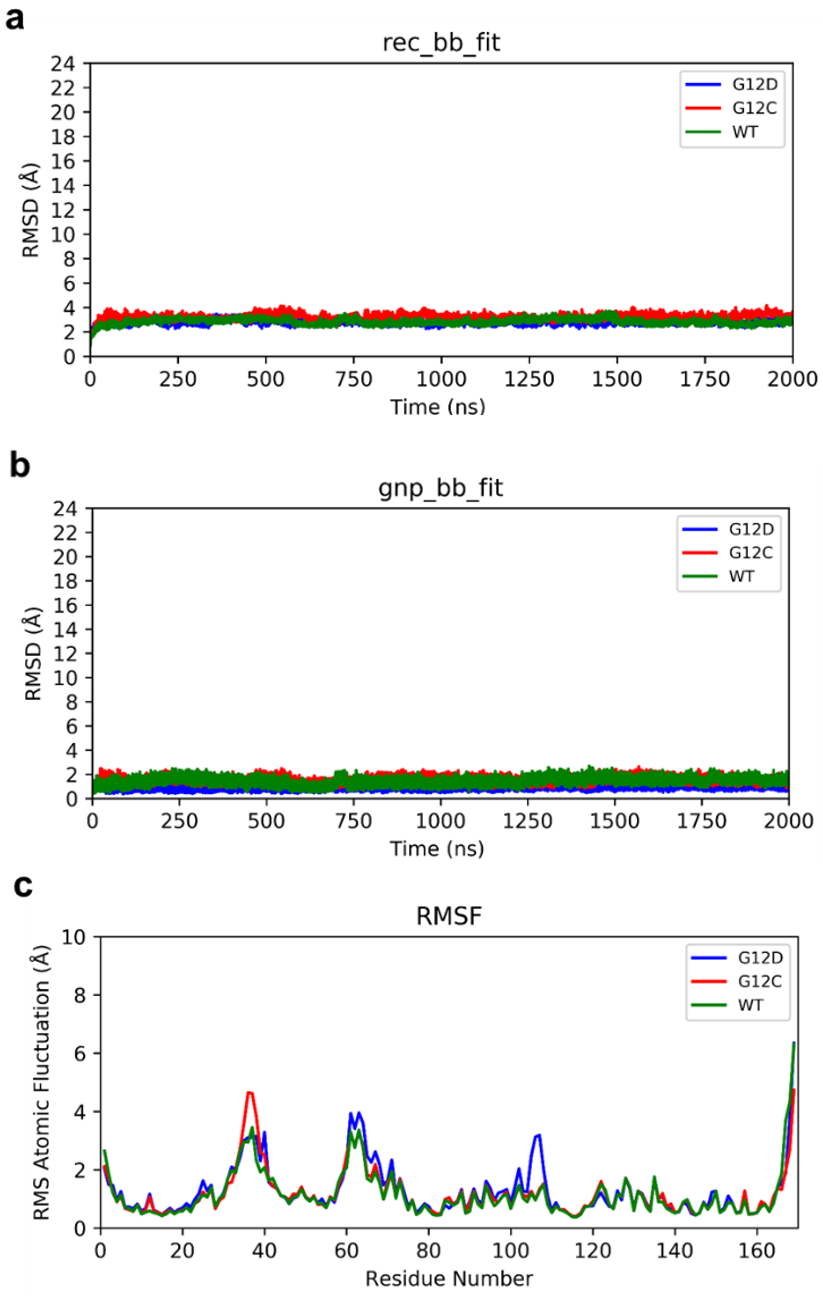

Figure 21. MDS trajectory analysis of mutant and wildtype KRAS. RMSD for KRAS protein backbones (G12D, G12C and WT) (**a**) and GppNHp (**b**) were plotted for 2 µs MDS**.** Atomic fluctuations, RMSF for all amino acid residue for KRAS proteins for 2 µs MDS were calculated and plotted (**c**).

This flexibility of KRAS4b G12D may translate to subtle differences in effector engagement. X-ray crystallography structures of KRAS bound to RAF1 RBDCRD (52-

188) reveal the RBD to interact solely with the switch I region of KRAS by forming an extended β-sheet structure, and the CRD to form hydrogen bonds and hydrophobic interactions with the inter-switch region (residues 41-48) and c-terminal α5 helix of KRAS (149, 153, and 157) (Tran et al., 2021). In contrast, there is no available structure of RAS bound to p110α, so no certain conclusions between mutant structural differences and p110α binding can be drawn. However, one study crystalized the oncogenic HRAS G12V protein bound to a truncated p110γ missing the adapter binding domain (ABD) and carrying the high affinity V223K mutation (Pacold et al., 2000). Eleven p110γ residues formed contacts with switch I of HRAS. Importantly, residue K234 was shown to interact with E63 and Y64 of HRAS's switch II region, making p110γ the first RAS effector identified to interact with both switch I and switch II of RAS (Figure 22a) (Pacold et al., 2000).

It is possible that alterations in switch II conformation influence the propensity for p110α binding. The KRAS G12R mutation is shown to bind to p110γ, but fails to engage p110α (Hobbs et al., 2020). A crystal structure of KRAS4b G12R-GMPPNP revealed no conformational change in switch I, but significant changes in switch II, including a partially unfolded α2 helix with only one helical turn instead of four (Hobbs et al., 2020). Although no clear causation can be drawn yet, the structural perturbation of switch II in KRAS G12R in conjunction with p110α binding ablation strongly suggests a role of this region in p110α binding. When returning to our doxycycline-inducible HeLa system, a Y64G mutation within the switch II region of KRAS4b was found to ablate KRAS4b G12D-induced AKT phosphorylation, but had little effect on ERK phosphorylation,

providing further evidence for the importance of this region in PI3Kinase engagement (Figure 22b).

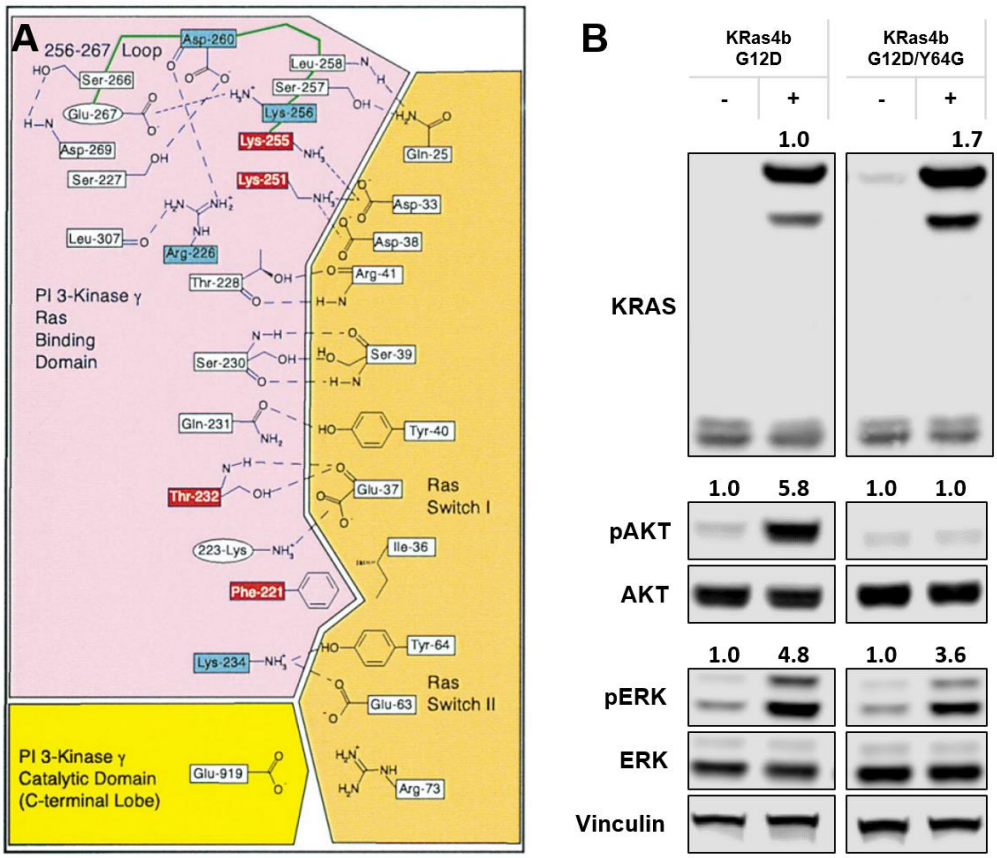

Figure 22. KRAS switch II is involved in p110α binding. Crystal structure contacts formed by HRAS G12V and truncated p110γ proteins lacking the ABD domain and carrying the high affinity V223K mutation (**a**). Figure adapted from Pacould et al., 2000. Evaluation of downstream RAS signaling by western blot of two doxycycline-induced HeLa cell lines expressing GFP-tagged KRAS4b G12D or KRAS4b G12D/Y64G. Plus and minus signs indicate the presence or absence of doxycycline (**b**)

Differential switch II dynamics may also influence GAP and GEF association, as both regulator proteins engage switch II during binding (Scheffzek et al., 1997; Boriack-Sjodin et al., 1998). Indeed, Hunter et al. found KRAS G12D to have the fastest GAP-stimulated hydrolysis rate when compared to G12A, G12C, G12R, G12V, G13D, Q61L,

and Q61H (2015). Subtle conformational differences in switch II may be responsible for this increased interaction, and may affect the proportion of active KRAS G12D (in a GAP concentration-dependent manner) and subsequently its oncogenic fitness.

While we did not observe significant differences in effector affinity for either p110α or RAF1(52-188) as measured by our BRET saturation curve system, we did see greater p110α engagement by mVenus- or GFP-tagged KRAS4b G12D through GFP immunoprecipitation experiments in HEK293T cells and dox-inducible HeLa cell lines. We also saw a greater relative increase in AKT activation with a GFP-KRAS4b G12D-driven HeLa cell line compared to the G12C mutant and wildtype proteins, and more p110α pulled down with GFP-KRAS G12D relative to G12C and WT. A panel of oncogenic cell lines also revealed higher AKT phosphorylation in G12D-driven lines compared to G12C-, G12V-, and G12R-mutant lines.

It is important to note the tissue-specific nature of effector engagement and dependence on oncogenic KRAS alleles. RAF1 is necessary for KRAS G12D-driven NSCLC, but not for KRAS G12D-driven PDAC formation (Eser et al., 2013). Additionally, deletion of the PI3K effector PDK1 prevents KRAS G12D-induced PDAC, but not KRAS G12D-driven NSCLC (Eser et al., 2013). Differences in effector expression levels, pathway activation and dependence, and signaling crosstalk all influence cellular protein-protein interactions. With their constitutively active PI3K pathway, HEK293T cells may not be the ideal system to interrogate p110α interactions, regardless of their excellent transfection capability and high protein output, which make them an efficient choice for assay development.

Additionally, it may be more difficult to detect differences in KRAS-p110α binding within a cellular context because p110α is recruited to the membrane through means ulterior to RAS. Relative to RAF1, which is held in an inactive complex in the cytosol prior to recruitment and activation by RAS binding, p110α associates with regulatory subunits containing two SH2 domains that bind to phosphotyrosyl residues on growth factor receptors, and is directly recruited by RTK signaling (Fruman et al., 2017). The catalytic-regulatory subunit complex can also be activated by heterotrimeric G proteins in the membrane (Fruman et al., 2017). Therefore, it is likely that p110α resides on the membrane in greater proportion or for a greater length of time than RAF1, which may hinder the detection of subtle differences in binding affinity between mutants in our BRET system.

While we were unable to determine significant differences in p110α or RAF1 RBDCRD engagement between oncogenic mutants KRAS G12C and G12D in our cellular BRET system, our finding of greater AKT signaling through the G12D mutant may still have therapeutic implications. G12D-specific inhibitors currently in development may hold greater efficacy in combination with PI3K pathway inhibitors if this mutation does have a greater dependence on this pathway. Additionally, while the lack of a clear difference between effector binding was disappointing, our BRET system can still be employed as a drug screening platform. If a single concentration of mVenus-KRAS and NanoLuc-tagged effector is transfected that corresponds to the BRET80 value of the pair's saturation curve, addition of drug in increasing concentrations would disrupt the BRET interaction, leading to a reduction in signal and a dose response curve. From

there, IC50 values could be extrapolated, and drug candidates could be evaluated for their ability to disrupt effector binding.

While there still exists no clear biochemical data detailing mutant-specific p110α binding, future SPR experiments with p110α and KRAS mutants may uncover subtle differences in affinity that are difficult to distinguish within our cellular BRET system. Incorporation of synthetic lipids with the use of nanodiscs would make for a stronger comparison by accounting for contacts between membrane lipids, full-length KRAS4b, and p110α. Additionally, solution-state NMR structures of KRAS4b G12C and G12D bound to the native nucleotide GTP would remove any artefacts related to synthetic GTP-analogs, and would either affirm initial findings or reveal additional differential switch perturbations between mutant KRAS proteins. Future solution state NMR studies will also investigate protein binding behavior with effector RBDs. We will also continue our evaluation of cellular p110α-KRAS binding by generating a panel of oncogenic cell lines with an affinity FLAG tag CRISPRed into the endogenous locus. Cell lines will be evaluated for differences in nucleotide loading and effector/interactor engagement.

CONCLUSIONS

The connection between RAS mutational frequency and biochemical properties remains unclear despite extensive efforts. Existing biochemical data report conflicting results, and although we did find GppNHp-bound KRAS4b G12D to have more flexibility in the switch II region than KRAS4b G12C, we were unable to determine mutant-specific preferences for effectors RAF1(52-188) and p110α in a cellular BRET approach. Indeed, within the complexities of a biological system, the consequences of RAS mutant biochemical properties are difficult to discern; RAS mutational frequency in cancers is influenced by a multitude of other factors, including mutagen exposure, signaling feedback modulation, tissue-specific effector concentrations, and the tumor microenvironment. However, we did establish a greater degree of binding to endogenous p110α by GFP-KRAS4b G12D compared to GFP-KRAS4b G12C and GFP-KRAS4b wildtype in both transiently transfected HEK293T cells and doxycycline-inducible HeLa cell lines by GFP pull-down. We also found higher induction of pAKT by GFP-KRAS4b G12D HeLas compared to GFP-KRAS4b G12C and GFP-KRAS4b wildtype. Additionally, a panel of oncogenic cell lines showed greater AKT phosphorylation in G12D-mutant lines compared to lines with G12C, G12V, and G12R mutations.

It may be that subtle differences in p110α binding between RAS mutants are difficult to discern using our BRET system, possibly because p110α resides at the membrane in a greater proportion due to its recruitment by means ulterior to RAS. Additionally, HEK293Ts may not be the ideal system for such a comparison, as their transduction with the large T antigen of SV40 maintains constitutive activation of the

PI3K pathway. Regardless, this optimized BRET system can be utilized as a drug screening platform in the search for mutant-specific RAS therapeutics. Additionally, if established, stronger PI3K signaling by G12D-mutant cancers has implications for patient treatment; G12D-specific therapies currently in development may be most effective in combination with a PI3K inhibitor.

We hope to further investigate whether the structural differences that we uncovered translate to downstream signaling through NMR and SPR experiments, and by generation and evaluation of a panel of oncogenic cell lines with an affinity FLAG tag CRISPRed into the endogenous locus. We aim to continue our contribution to the understanding of RAS-driven cancers, and to build on the RAS community's momentum to eradicate RAS-driven diseases.

REFERENCES

Ahmadian, M. R., P. Stege, K. Scheffzek, and A. Wittinghofer. 1997. Confirmation of the arginine-finger hypothesis for the GAP-stimulated GTP-hydrolysis reaction of Ras. Nature structural biology 4(9):686-689.

Ayoub, M. A., A. Levoye, P. Delagrange, and R. Jockers. 2004. Preferential formation of MT1/MT2 melatonin receptor heterodimers with distinct ligand interaction properties compared with MT2 homodimers. Molecular pharmacology 66(2):312-321.

Bader, A. G., S. Kang, and P. K. Vogt. 2006. Cancer-specific mutations in PIK3CA are oncogenic in vivo. Proceedings of the National Academy of Sciences 103(5):1475-1479.

Bivona, T. G., S. E. Quatela, B. O. Bodemann, I. M. Ahearn, M. J. Soskis, A. Mor, J. Miura, H. H. Wiener, L. Wright, and S. G. Saba. 2006. PKC regulates a farnesyl-electrostatic switch on K-Ras that promotes its association with Bcl-XL on mitochondria and induces apoptosis. Molecular cell 21(4):481-493.

Bondeva, T., A. Balla, P. Várnai, and T. Balla. 2002. Structural determinants of Ras-Raf interaction analyzed in live cells. Molecular biology of the cell 13(7):2323-2333.

Boriack-Sjodin, P. A., S. Margarit, D. Bar-Sagi, and J. Kuriyan. 1998. The structural basis of the activation of Ras by Sos. Nature 394(6691):337-343.

Bos, J. L., H. Rehmann, and A. Wittinghofer. 2007. GEFs and GAPs: Critical Elements in the Control of Small G Proteins. Cell 129(5):865-877. doi: https://doi.org/10.1016/j.cell.2007.05.018

Breit, A., M. Lagacé, and M. Bouvier. 2004. Hetero-oligomerization between β2-and β3-adrenergic receptors generates a β-adrenergic signaling unit with distinct functional properties. Journal of Biological Chemistry 279(27):28756-28765.

Burge, R. A., and G. A. Hobbs. 2022. Not all RAS mutations are equal: A detailed review of the functional diversity of RAS hot spot mutations. RAS: Past, Present, and Future:29.

Castellano, E., and J. Downward. 2011. RAS interaction with PI3K: more than just another effector pathway. Genes & cancer 2(3):261-274.

Céspedes, M. V., F. J. Sancho, S. Guerrero, M. Parreño, I. Casanova, M. A. Pavón, E. Marcuello, M. Trias, M. Cascante, and G. Capellà. 2006. K-ras Asp12 mutant neither interacts with Raf, nor signals through Erk and is less tumorigenic than K-ras Val12. Carcinogenesis 27(11):2190-2200.

Chandra, A., H. E. Grecco, V. Pisupati, D. Perera, L. Cassidy, F. Skoulidis, S. A. Ismail, C. Hedberg, M. Hanzal-Bayer, and A. R. Venkitaraman. 2012. The GDI-like solubilizing factor PDEδ sustains the spatial organization and signalling of Ras family proteins. Nature cell biology 14(2):148-158.

Christensen, J. G. 2021. Discovery and characterization of MRTX1133, a selective non-covalent inhibitor of KRASG12D. In: Paper presented at: AACR-NCI-EORTC Virtual International Conference on Molecular Targets and Cancer Therapeutics

Cook, J. H., G. E. Melloni, D. C. Gulhan, P. J. Park, and K. M. Haigis. 2021. The origins and genetic interactions of KRAS mutations are allele-and tissue-specific. Nature communications 12(1):1-14.

Dent, P., D. B. Reardon, D. K. Morrison, and T. W. Sturgill. 1995. Regulation of Raf-1 and Raf-1 mutants by Ras-dependent and Ras-independent mechanisms in vitro. Molecular and Cellular Biology 15(8):4125-4135.

Der, C. J., T. Finkel, and G. M. Cooper. 1986. Biological and biochemical properties of human rasH genes mutated at codon 61. Cell 44(1):167-176.
Diehl, A., L. M. Hannan, and E. G. Chiorean. 2021. Prognostic value of KRAS and PI3K pathway mutations for advanced pancreatic ductal adenocarcinoma (PDAC) patients (pts). American Society of Clinical Oncology.
Ebrahimi, S., M. Hosseini, S. Shahidsales, M. Maftouh, G. A Ferns, M. Ghayour-Mobarhan, S. Mahdi Hassanian, and A. Avan. 2017. Targeting the Akt/PI3K signaling pathway as a potential therapeutic strategy for the treatment of pancreatic cancer. Current medicinal chemistry 24(13):1321-1331.
Eser, S., N. Reiff, M. Messer, B. Seidler, K. Gottschalk, M. Dobler, M. Hieber, A. Arbeiter, S. Klein, and B. Kong. 2013. Selective requirement of PI3K/PDK1 signaling for Kras oncogene-driven pancreatic cell plasticity and cancer. Cancer cell 23(3):406-420.
Esteban, L. M., C. Vicario-Abejón, P. Fernández-Salguero, A. Fernández-Medarde, N. Swaminathan, K. Yienger, E. Lopez, M. Malumbres, R. McKay, and J. M. Ward. 2001. Targeted genomic disruption of H-ras and N-ras, individually or in combination, reveals the dispensability of both loci for mouse growth and development. Molecular and cellular biology 21(5):1444-1452.
Fasano, O., T. Aldrich, F. Tamanoi, E. Taparowsky, M. Furth, and M. Wigler. 1984. Analysis of the transforming potential of the human H-ras gene by random mutagenesis. Proceedings of the National Academy of Sciences 81(13):4008-4012.
Ferro, E., and L. Trabalzini. 2010. RalGDS family members couple Ras to Ral signalling and that's not all. Cellular signalling 22(12):1804-1810.
Fisher, G. H., S. L. Wellen, D. Klimstra, J. M. Lenczowski, J. W. Tichelaar, M. J. Lizak, J. A. Whitsett, A. Koretsky, and H. E. Varmus. 2001. Induction and apoptotic regression of lung adenocarcinomas by regulation of a K-Ras transgene in the presence and absence of tumor suppressor genes. Genes & development 15(24):3249-3262.
Floyd, H. S., C. L. Farnsworth, N. D. Kock, M. C. Mizesko, J. L. Little, S. T. Dance, J. Everitt, J. Tichelaar, J. A. Whitsett, and M. S. Miller. 2005. Conditional expression of the mutant Ki-ras G12C allele results in formation of benign lung adenomas: Development of a novel mouse lung tumor model. Carcinogenesis 26(12):2196-2206.
Ford, B., K. Skowronek, S. Boykevisch, D. Bar-Sagi, and N. Nassar. 2005. Structure of the G60A Mutant of Ras: IMPLICATIONS FOR THE DOMINANTNEGATIVEEFFECT. Journal of Biological Chemistry 280(27):25697-25705.
Fruman, D. A., H. Chiu, B. D. Hopkins, S. Bagrodia, L. C. Cantley, and R. T. Abraham. 2017. The PI3K pathway in human disease. Cell 170(4):605-635.
Fruman, D. A., R. E. Meyers, and L. C. Cantley. 1998. Phosphoinositide kinases. Annual review of biochemistry 67:481.
Gasper, R., and F. Wittinghofer. 2020. The Ras switch in structural and historical perspective. Biological chemistry 401(1):143-163.
Gillies, T. E., M. Pargett, J. M. Silva, C. K. Teragawa, F. McCormick, and J. G. Albeck. 2020. Oncogenic mutant RAS signaling activity is rescaled by the ERK/MAPK pathway. Molecular systems biology 16(10):e9518.
Gressani, K. M., S. Leone-Kabler, M. G. O'Sullivan, L. D. Case, A. M. Malkinson, and M. S. Miller. 1999. Strain-dependent lung tumor formation in mice transplacentally exposed to 3-methylcholanthrene and post-natally exposed to butylated hydroxytoluene. Carcinogenesis 20(11):2159-2165.

Gupta, S., A. R. Ramjaun, P. Haiko, Y. Wang, P. H. Warne, B. Nicke, E. Nye, G. Stamp, K. Alitalo, and J. Downward. 2007. Binding of ras to phosphoinositide 3-kinase p110α is required for ras-driven tumorigenesis in mice. Cell 129(5):957-968.

Gutierrez, L., A. Magee, C. Marshall, and J. Hancock. 1989. Post-translational processing of p21ras is two-step and involves carboxyl-methylation and carboxy-terminal proteolysis. The EMBO journal 8(4):1093-1098.

Gymnopoulos, M., M.-A. Elsliger, and P. K. Vogt. 2007. Rare cancer-specific mutations in PIK3CA show gain of function. Proceedings of the National Academy of Sciences 104(13):5569-5574.

Haigis, K. M., K. R. Kendall, Y. Wang, A. Cheung, M. C. Haigis, J. N. Glickman, M. Niwa-Kawakita, A. Sweet-Cordero, J. Sebolt-Leopold, and K. M. Shannon. 2008. Differential effects of oncogenic K-Ras and N-Ras on proliferation, differentiation and tumor progression in the colon. Nature genetics 40(5):600-608.

Hall, M. P., J. Unch, B. F. Binkowski, M. P. Valley, B. L. Butler, M. G. Wood, P. Otto, K. Zimmerman, G. Vidugiris, and T. Machleidt. 2012. Engineered luciferase reporter from a deep sea shrimp utilizing a novel imidazopyrazinone substrate. ACS chemical biology 7(11):1848-1857.

Hancock, J. F., A. I. Magee, J. E. Childs, and C. J. Marshall. 1989. All ras proteins are polyisoprenylated but only some are palmitoylated. Cell 57(7):1167-1177.

Hancock, J. F., H. Paterson, and C. J. Marshall. 1990. A polybasic domain or palmitoylation is required in addition to the CAAX motif to localize p21ras to the plasma membrane. Cell 63(1):133-139.

Hobbs, G. A., N. M. Baker, A. M. Miermont, R. D. Thurman, M. Pierobon, T. H. Tran, A. O. Anderson, A. M. Waters, J. N. Diehl, and B. Papke. 2020. Atypical KRASG12R mutant is impaired in PI3K signaling and macropinocytosis in pancreatic cancer. Cancer discovery 10(1):104-123.

Hobbs, G. A., and C. J. Der. 2019. RAS mutations are not created equal. Cancer discovery 9(6):696-698.

Hunter, J. C., A. Manandhar, M. A. Carrasco, D. Gurbani, S. Gondi, and K. D. Westover. 2015. Biochemical and structural analysis of common cancer-associated KRAS mutations. Molecular cancer research 13(9):1325-1335.

Hwang, M.-C. C., Y.-J. Sung, and Y.-W. Hwang. 1996. The differential effects of the Gly-60 to Ala mutation on the interaction of H-Ras p21 with different downstream targets. Journal of Biological Chemistry 271(14):8196-8202.

Ihle, N. T., L. A. Byers, E. S. Kim, P. Saintigny, J. J. Lee, G. R. Blumenschein, A. Tsao, S. Liu, J. E. Larsen, and J. Wang. 2012. Effect of KRAS oncogene substitutions on protein behavior: implications for signaling and clinical outcome. Journal of the National Cancer Institute 104(3):228-239.

Isakoff, S. J., J. A. Engelman, H. Y. Irie, J. Luo, S. M. Brachmann, R. V. Pearline, L. C. Cantley, and J. S. Brugge. 2005. Breast cancer–associated PIK3CA mutations are oncogenic in mammary epithelial cells. Cancer research 65(23):10992-11000.

Jackson, E. L., N. Willis, K. Mercer, R. T. Bronson, D. Crowley, R. Montoya, T. Jacks, and D. A. Tuveson. 2001. Analysis of lung tumor initiation and progression using conditional expression of oncogenic K-ras. Genes & development 15(24):3243-3248.

Jennings-Gee, J. E., J. E. Moore, M. Xu, S. T. Dance, N. D. Kock, T. P. McCoy, J. J. Carr, and M. S. Miller. 2006. Strain-specific induction of murine lung tumors following in utero exposure to 3-methylcholanthrene. Molecular Carcinogenesis: Published in cooperation with the University of Texas MD Anderson Cancer Center 45(9):676-684.

Johnson, L., D. Greenbaum, K. Cichowski, K. Mercer, E. Murphy, E. Schmitt, R. T. Bronson, H. Umanoff, W. Edelmann, and R. Kucherlapati. 1997. K-ras is an essential gene in the mouse with partial functional overlap with N-ras. Genes & development 11(19):2468-2481.

Johnson, L., K. Mercer, D. Greenbaum, R. T. Bronson, D. Crowley, D. A. Tuveson, and T. Jacks. 2001. Somatic activation of the K-ras oncogene causes early onset lung cancer in mice. Nature 410(6832):1111-1116.

Jura, N., E. Scotto-Lavino, A. Sobczyk, and D. Bar-Sagi. 2006. Differential modification of Ras proteins by ubiquitination. Molecular cell 21(5):679-687.

Kiel, C., D. Matallanas, and W. Kolch. 2021. The ins and outs of RAS effector complexes. Biomolecules 11(2):236.

Koera, K., K. Nakamura, K. Nakao, J. Miyoshi, K. Toyoshima, T. Hatta, H. Otani, A. Aiba, and M. Katsuki. 1997. K-ras is essential for the development of the mouse embryo. Oncogene 15(10):1151-1159.

Kremers, G.-J., J. Goedhart, E. B. van Munster, and T. W. Gadella. 2006. Cyan and yellow super fluorescent proteins with improved brightness, protein folding, and FRET Förster radius. Biochemistry 45(21):6570-6580.

Laude, A. J., and I. A. Prior. 2008. Palmitoylation and localisation of RAS isoforms are modulated by the hypervariable linker domain. Journal of cell science 121(4):421-427.

Leone-Kabler, S., L. L. Wessner, M. F. McEntee, R. D'Agostino Jr, and M. Miller. 1997. Ki-ras mutations are an early event and correlate with tumor stage in transplacentally-induced murine lung tumors. Carcinogenesis 18(6):1163-1168.

Li, S., A. Balmain, and C. M. Counter. 2018. A model for RAS mutation patterns in cancers: finding the sweet spot. Nature Reviews Cancer 18(12):767-777.

Lim, K.-H., and C. M. Counter. 2005. Reduction in the requirement of oncogenic Ras signaling to activation of PI3K/AKT pathway during tumor maintenance. Cancer cell 8(5):381-392.

Liu, J., R. Kang, and D. Tang. 2021. The KRAS-G12c inhibitor: activity and resistance. p 1-4. Nature Publishing Group.

Menzies, G. E., I. A. Prior, A. Brancale, S. H. Reed, and P. D. Lewis. 2021. Carcinogen-induced DNA structural distortion differences in the RAS gene isoforms; the importance of local sequence. BMC chemistry 15(1):1-13.

Mercier, J.-F., A. Salahpour, S. Angers, A. Breit, and M. Bouvier. 2002. Quantitative assessment of β1-and β2-adrenergic receptor homo-and heterodimerization by bioluminescence resonance energy transfer. Journal of Biological Chemistry 277(47):44925-44931.

Meuwissen, R., S. C. Linn, M. van der Valk, W. J. Mooi, and A. Berns. 2001. Mouse model for lung tumorigenesis through Cre/lox controlled sporadic activation of the K-Ras oncogene. Oncogene 20(45):6551-6558.

Milburn, M. V., L. Tong, A. M. DeVos, A. Brünger, Z. Yamaizumi, S. Nishimura, and S.-H. Kim. 1990. Molecular switch for signal transduction: structural differences between active and inactive forms of protooncogenic ras proteins. Science 247(4945):939-945.

Mo, X.-L., and H. Fu. 2016. BRET: NanoLuc-based bioluminescence resonance energy transfer platform to monitor protein-protein interactions in live cells, High Throughput Screening. Springer. p. 263-271.

Moore, A. R., S. C. Rosenberg, F. McCormick, and S. Malek. 2020. RAS-targeted therapies: is the undruggable drugged? Nature Reviews Drug Discovery 19(8):533-552.

Morrison, D. K., D. R. Kaplan, U. Rapp, and T. M. Roberts. 1988. Signal transduction from membrane to cytoplasm: growth factors and membrane-bound oncogene products

increase Raf-1 phosphorylation and associated protein kinase activity. Proceedings of the National Academy of Sciences 85(23):8855-8859.
Muraoka, S., F. Shima, M. Araki, T. Inoue, A. Yoshimoto, Y. Ijiri, N. Seki, A. Tamura, T. Kumasaka, and M. Yamamoto. 2012. Crystal structures of the state 1 conformations of the GTP-bound H-Ras protein and its oncogenic G12V and Q61L mutants. FEBS letters 586(12):1715-1718.
Pacold, M. E., S. Suire, O. Perisic, S. Lara-Gonzalez, C. T. Davis, E. H. Walker, P. T. Hawkins, L. Stephens, J. F. Eccleston, and R. L. Williams. 2000. Crystal structure and functional analysis of Ras binding to its effector phosphoinositide 3-kinase γ. Cell 103(6):931-944.
Pálfy, G., I. Vida, and A. Perczel. 2020. 1H, 15N backbone assignment and comparative analysis of the wild type and G12C, G12D, G12V mutants of K-Ras bound to GDP at physiological pH. Biomolecular NMR Assignments 14(1):1-7.
Pearson, G., F. Robinson, T. Beers Gibson, B.-e. Xu, M. Karandikar, K. Berman, and M. H. Cobb. 2001. Mitogen-activated protein (MAP) kinase pathways: regulation and physiological functions. Endocrine reviews 22(2):153-183.
Pershing, N. L., B. L. Lampson, J. A. Belsky, E. Kaltenbrun, D. M. MacAlpine, and C. M. Counter. 2015. Rare codons capacitate Kras-driven de novo tumorigenesis. The Journal of clinical investigation 125(1):222-233.
Pfleger, K. D., and K. A. Eidne. 2006. Illuminating insights into protein-protein interactions using bioluminescence resonance energy transfer (BRET). Nature methods 3(3):165-174.
Potenza, N., C. Vecchione, A. Notte, A. De Rienzo, A. Rosica, L. Bauer, A. Affuso, M. De Felice, T. Russo, and R. Poulet. 2005. Replacement of K-Ras with H-Ras supports normal embryonic development despite inducing cardiovascular pathology in adult mice. EMBO reports 6(5):432-437.
Prior, I. A., F. E. Hood, and J. L. Hartley. 2020. The frequency of Ras mutations in cancer. Cancer research 80(14):2969-2974.
Prior, I. A., P. D. Lewis, and C. Mattos. 2012. A comprehensive survey of Ras mutations in cancer. Cancer research 72(10):2457-2467.
Rabara, D., T. H. Tran, S. Dharmaiah, R. M. Stephens, F. McCormick, D. K. Simanshu, and M. Holderfield. 2019. KRAS G13D sensitivity to neurofibromin-mediated GTP hydrolysis. Proceedings of the National Academy of Sciences 116(44):22122-22131.
Ramakrishnan, G., G. Davaakhuu, L. Kaplun, W.-C. Chung, A. Rana, A. Atfi, L. Miele, and G. Tzivion. 2014. Sirt2 deacetylase is a novel AKT binding partner critical for AKT activation by insulin. Journal of Biological Chemistry 289(9):6054-6066.
Riquelme, E., C. Behrens, H. Y. Lin, G. Simon, V. Papadimitrakopoulou, J. Izzo, C. Moran, N. Kalhor, J. J. Lee, and J. D. Minna. 2016. Modulation of EZH2 Expression by MEK-ERK or PI3K-AKT Signaling in Lung Cancer Is Dictated by Different KRAS Oncogene MutationsOncogenic KRAS Modulates EZH2 Expression in NSCLC. Cancer research 76(3):675-685.
Ritt, D. A., M. Zhou, T. P. Conrads, T. D. Veenstra, T. D. Copeland, and D. K. Morrison. 2007. CK2 Is a component of the KSR1 scaffold complex that contributes to Raf kinase activation. Current biology 17(2):179-184.
Rocks, O., A. Peyker, M. Kahms, P. J. Verveer, C. Koerner, M. Lumbierres, J. Kuhlmann, H. Waldmann, A. Wittinghofer, and P. I. Bastiaens. 2005. An acylation cycle regulates localization and activity of palmitoylated Ras isoforms. Science 307(5716):1746-1752.
Rodriguez-Viciana, P., J. Oses-Prieto, A. Burlingame, M. Fried, and F. McCormick. 2006. A phosphatase holoenzyme comprised of Shoc2/Sur8 and the catalytic subunit of PP1 functions as an M-Ras effector to modulate Raf activity. Molecular cell 22(2):217-230.

Rosseland, C. M., L. Wierød, L. I. Flinder, M. P. Oksvold, E. Skarpen, and H. S. Huitfeldt. 2008. Distinct functions of H-Ras and K-Ras in proliferation and survival of primary hepatocytes due to selective activation of ERK and PI3K. Journal of cellular physiology 215(3):818-826.

Samuels, Y., L. A. Diaz Jr, O. Schmidt-Kittler, J. M. Cummins, L. DeLong, I. Cheong, C. Rago, D. L. Huso, C. Lengauer, and K. W. Kinzler. 2005. Mutant PIK3CA promotes cell growth and invasion of human cancer cells. Cancer cell 7(6):561-573.

Samuels, Y., Z. Wang, A. Bardelli, N. Silliman, J. Ptak, S. Szabo, H. Yan, A. Gazdar, S. M. Powell, and G. J. Riggins. 2004. High frequency of mutations of the PIK3CA gene in human cancers. Science 304(5670):554-554.

Sarkozy, A., C. Carta, S. Moretti, G. Zampino, M. C. Digilio, F. Pantaleoni, A. P. Scioletti, G. Esposito, V. Cordeddu, and F. Lepri. 2009. Germline BRAF mutations in Noonan, LEOPARD, and cardiofaciocutaneous syndromes: molecular diversity and associated phenotypic spectrum. Human mutation 30(4):695-702.

Scheffzek, K., M. R. Ahmadian, W. Kabsch, L. Wiesmuller, A. Lautwein, F. Schmitz, and A. Wittinghofer. 1997. The Ras-RasGAP complex: structural basis for GTPase activation and its loss in oncogenic Ras mutants. Science 277(5324):333-339.

Schneider, C. A., W. S. Rasband, and K. W. Eliceiri. 2012. NIH Image to ImageJ: 25 years of image analysis. Nature methods 9(7):671-675.

Seeburg, P. H., W. W. Colby, D. J. Capon, D. V. Goeddel, and A. D. Levinson. 1984. Biological properties of human c-Ha-ras1 genes mutated at codon 12. Nature 312(5989):71-75.

Simanshu, D. K., D. V. Nissley, and F. McCormick. 2017. RAS proteins and their regulators in human disease. Cell 170(1):17-33.

Spoerner, M., C. Herrmann, I. R. Vetter, H. R. Kalbitzer, and A. Wittinghofer. 2001. Dynamic properties of the Ras switch I region and its importance for binding to effectors. Proceedings of the National Academy of Sciences 98(9):4944-4949.

Stolze, B., S. Reinhart, L. Bulllinger, S. Fröhling, and C. Scholl. 2015. Comparative analysis of KRAS codon 12, 13, 18, 61 and 117 mutations using human MCF10A isogenic cell lines. Scientific reports 5(1):1-9.

Swarthout, J. T., S. Lobo, L. Farh, M. R. Croke, W. K. Greentree, R. J. Deschenes, and M. E. Linder. 2005. DHHC9 and GCP16 constitute a human protein fatty acyltransferase with specificity for H-and N-Ras. Journal of Biological Chemistry 280(35):31141-31148.

Takai, Y., T. Sasaki, and T. Matozaki. 2001. Small GTP-binding proteins. Physiological reviews 81(1):153-208.

Terrell, E. M., and D. K. Morrison. 2019. Ras-mediated activation of the Raf family kinases. Cold Spring Harbor perspectives in medicine 9(1):a033746.

Terrillon, S., T. Durroux, B. Mouillac, A. Breit, M. A. Ayoub, M. Taulan, R. Jockers, C. Barberis, and M. Bouvier. 2003. Oxytocin and vasopressin V1a and V2 receptors form constitutive homo-and heterodimers during biosynthesis. Molecular endocrinology 17(4):677-691.

Tomasetti, C., and B. Vogelstein. 2015. Variation in cancer risk among tissues can be explained by the number of stem cell divisions. Science 347(6217):78-81.

Tran, T. H., A. H. Chan, L. C. Young, L. Bindu, C. Neale, S. Messing, S. Dharmaiah, T. Taylor, J.-P. Denson, and D. Esposito. 2021. KRAS interaction with RAF1 RAS-binding domain and cysteine-rich domain provides insights into RAS-mediated RAF activation. Nature communications 12(1):1-16.

Umanoff, H., W. Edelmann, A. Pellicer, and R. Kucherlapati. 1995. The murine N-ras gene is not essential for growth and development. Proceedings of the National Academy of Sciences 92(5):1709-1713.

Vetter, I. R., and A. Wittinghofer. 2001. The guanine nucleotide-binding switch in three dimensions. Science 294(5545):1299-1304.
Voice, J. K., R. L. Klemke, A. Le, and J. H. Jackson. 1999. Four human ras homologs differ in their abilities to activate Raf-1, induce transformation, and stimulate cell motility. Journal of Biological Chemistry 274(24):17164-17170.
Wall, V. E., L. A. Garvey, J. L. Mehalko, L. V. Procter, and D. Esposito. 2014. Combinatorial assembly of clone libraries using site-specific recombination, DNA Cloning and Assembly Methods. Springer. p. 193-208.
Wang, X., S. Allen, J. F. Blake, V. Bowcut, D. M. Briere, A. Calinisan, J. R. Dahlke, J. B. Fell, J. P. Fischer, and R. J. Gunn. 2021. Identification of MRTX1133, a Noncovalent, Potent, and Selective KRASG12D Inhibitor. Journal of medicinal chemistry
Weihs, F., J. Wang, K. D. Pfleger, and H. Dacres. 2020. Experimental determination of the bioluminescence resonance energy transfer (BRET) Förster distances of NanoBRET and red-shifted BRET pairs. Analytica chimica acta: X 6:100059.
Wilson, S., G. Wilkinson, and G. Milligan. 2005. The CXCR1 and CXCR2 receptors form constitutive homo-and heterodimers selectively and with equal apparent affinities. Journal of Biological Chemistry 280(31):28663-28674.
Wittinghofer, A., and E. F. Pal. 1991. The structure of Ras protein: a model for a universal molecular switch. Trends in biochemical sciences 16:382-387.
Zhang, Z., K. Z. Guiley, and K. M. Shokat. 2022a. Chemical acylation of an acquired serine suppresses oncogenic signaling of K-Ras (G12S). Nature chemical biology:1-7.
Zhang, Z., J. Morstein, A. K. Ecker, K. Z. Guiley, and K. M. Shokat. 2022b. Chemoselective covalent modification of K-Ras (G12R) with a small molecule electrophile. Journal of the American Chemical Society 144(35):15916-15921.
Zhao, L., and P. K. Vogt. 2010. Hot-spot mutations in p110α of phosphatidylinositol 3-kinase (PI3K): differential interactions with the regulatory subunit p85 and with RAS. Cell cycle 9(3):596-600.
Zheng, Q., D. M. Peacock, and K. M. Shokat. 2022. Drugging the Next Undruggable KRAS Allele-Gly12Asp. Journal of Medicinal Chemistry